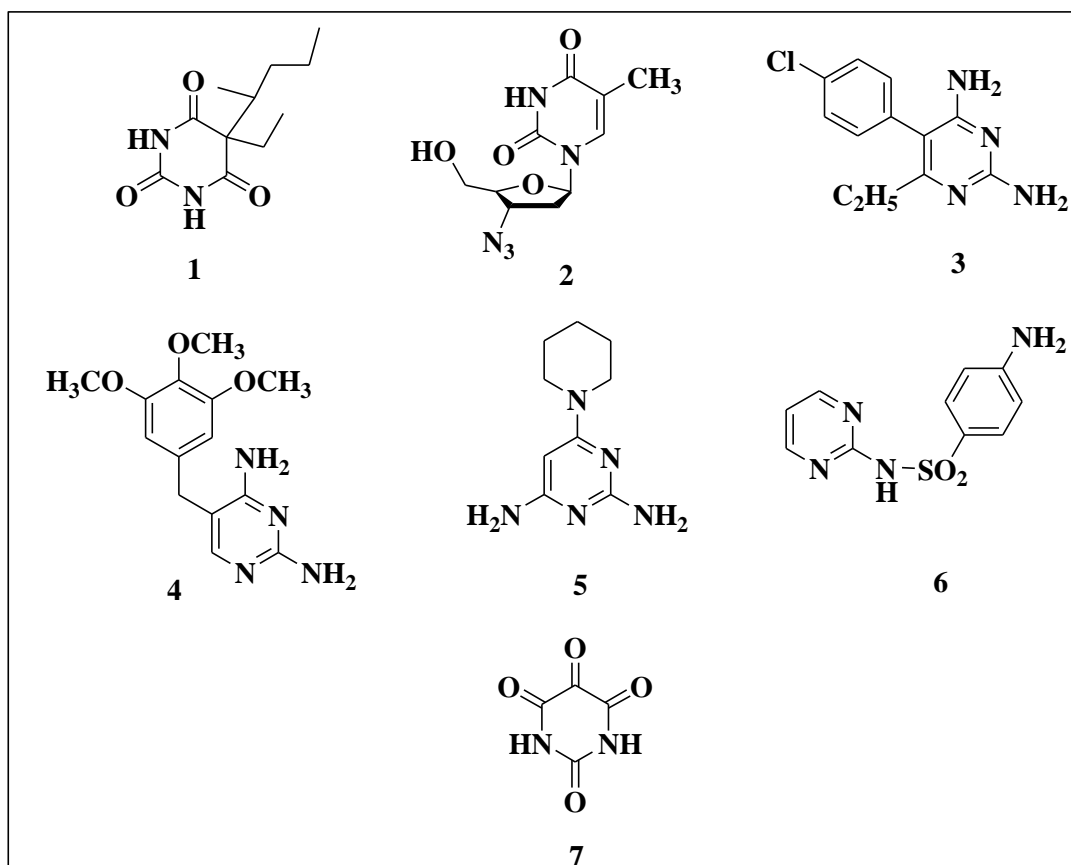


## *Chapter 3A*

**Literature on strategies for conversion of 3, 4-dihydropyrimidinones to pyrimidines**

### 3A.1. Pyrimidines and their synthesis from Biginelli 3, 4-dihydropyrimidin-2(1H)-ones

Pyrimidine is an aromatic heterocyclic compound containing two N-atoms at positions 1 and 3 of the six membered ring. It is also known as ‘*m*-diazine’. It has wide occurrence in nature as substituted and ring fused compounds and derivatives including the nucleotides, thiamine (vitamin B1) and alloxan. Over the years, this ring system turned out an important pharmacophore. It is found in many synthetic drugs such as barbiturates: thiopental sodium **1** (*Pentothal*), HIV drug zidovudine **2**. Some diaminopyrimidines (**Fig. 3A.1**), such as pyrimethamine **3** or trimethoprim **4** are potential antimalarial drugs. Minoxidil **5** can act as powerful antihypertensive whereas sulfadiazine **6** is one of the chemotherapeutics containing a pyrimidine moiety [1].



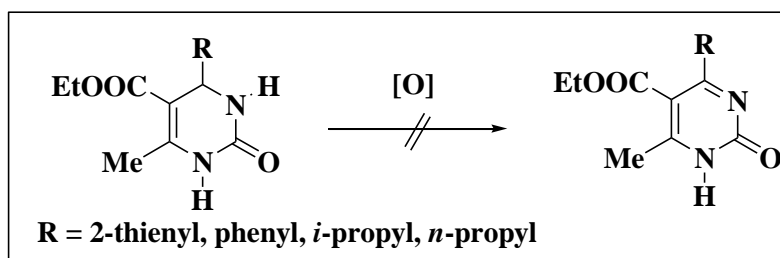
**Fig. 3A.1:** Structures of some bioactive pyrimidines

In earlier chapter we discussed about broad spectrum of biological activities of synthetic and natural pyrimidinone derivatives which include anticancer, anti-inflammatory, analgesic, anticonvulsant, antihelmintic, anti-allergic activity, calcium

channel modulators,  $\alpha_{1a}$ -adrenergic receptor antagonists, mitotic kinesin inhibitors, and hepatitis B virus replication inhibitors [1, 2]. The well-known Biginelli 3,4-dihydropyrimidin-2(*IH*)-ones (DHPMs) are chemical precursors of multifunctionalized pyrimidines which are known for more than a century [3] prepared from the multicomponent reactions of aldehydes,  $\beta$ -ketoester and urea or thiourea molecules using acid catalyst as discussed in **Chapter 2B**. The wide spectrum of biological activity allows consideration of the dihydropyrimidin structural unit as one of the most drug-like scaffolds. However, there has been a lack of methodology to efficiently convert the Biginelli DHPMs to pyrimidines [4-6]. In this section, we have included a literature survey of various routes for conversion of the Biginelli DHPMs to multifunctionalized pyrimidines till date.

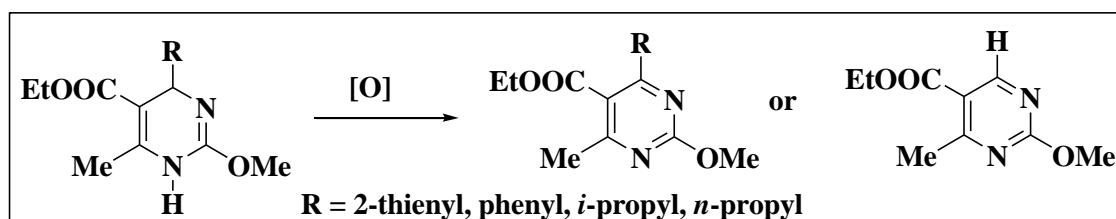
The most reported methods utilize a four step process to realize such a chemical transformation. The Biginelli DHPMs are sequentially dehydrogenated, tautomerized, activated and coupled with a nucleophile. Dehydrogenation of the Biginelli DHPMs is known to be exceedingly difficult [7-9]. The sensitivity of the methyl group at the C-6 position to some oxidizing agents such as  $\text{SeO}_2$  and the inertness of the DMPM ring toward a variety of oxidizing agents make the dehydrogenation very trouble. In the conversion of DHPMs to 2-substituted pyrimidines, the four step processes also include chlorination or sulfonylation reactions followed by coupling with a nucleophile. The use of toxic and corrosive reagents for chlorination or sulfonylation with sensitive functionalities at high temperature could be problematic if the sequential reactions are attempted in one pot [4-6]. Only few reports described the efficient conversion of Biginelli DHPMs units to pyrimidine derivatives through dehydrogenation reaction [7-9].

Many attempts to oxidize (i.e. dehydrogenate) DHPMs (**Scheme 3A.1**) with a number of different oxidation reagents and conditions failed. These DHPMs appeared to be quite stable towards  $\text{NaNO}_2$  in acetic acid [10], pyridinium chlorochromate [10], ceric ammonium nitrate [11],  $\text{MnO}_2$  [12-15],  $\text{KMnO}_4$  /clay [16], chloranil and DDQ [17, 18].



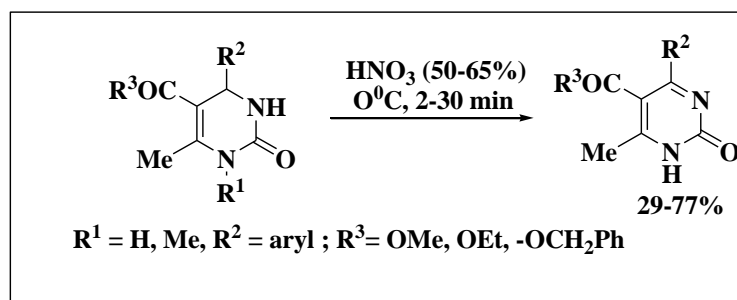
**Scheme 3A.1:** Unsuccessful attempt for oxidation of Biginelli 3, 4-dihydropyrimidinones

On the other hand, 1, 4-dihydropyrimidines readily dehydrogenated under most of the above conditions to yield the desired pyrimidines, or in some cases dealkylated (i.e. C4-unsubstituted) pyrimidine (**Scheme 3A.2**) [8].

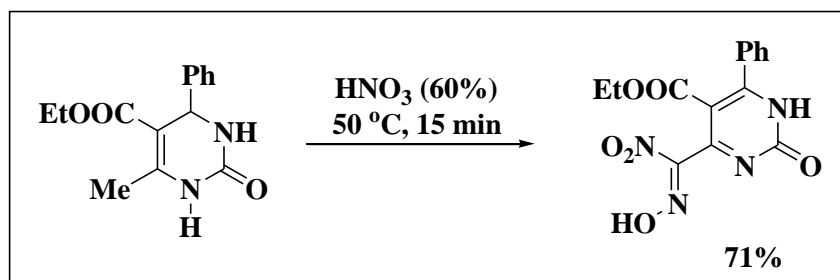


**Scheme 3A.2:** Dehydrogenation of 1, 4-dihydropyrimidines

Puchala et al. [9] explored the oxidative dehydrogenation of substituted 3,4-dihydro-2-pyrimidones (DHPMs) to 2-pyrimidinones in moderate to good yields using 50-65% of nitric acid at 0 °C (**Scheme 3A.3**). In contrast, reaction of one model DHPM with 60% nitric acid at 50 °C led to highly stable nitrolic acid, involving a formal nitration, nitrosation, and dehydrogenation step (**Scheme 3A.4**).



**Scheme 3A.3:** Dehydrogenation of substituted 3, 4-dihydro-2-pyrimidones (DHPMs) to 2-pyrimidinones

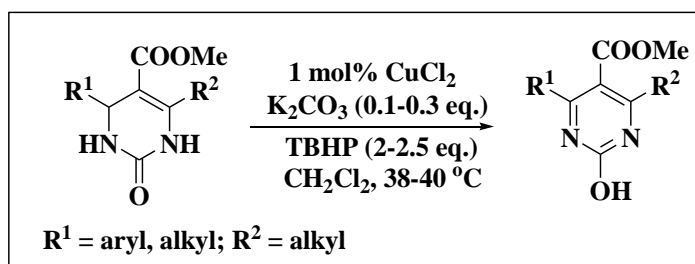


**Scheme 3A.4:** Conversion of DHPM to nitrolic acid

The lower solubility, steric effects of various substituents and electron deficient nature of phenyl rings of DHPMs mainly controlled the rate of dehydrogenation reactions.

Shanmugam et al. [19] overcame the above mentioned limitations of DHPMs oxidation by the ceric ammonium nitrate (CAN) solution in water at room temperature stirring for 12 h with varieties of DHPMs.

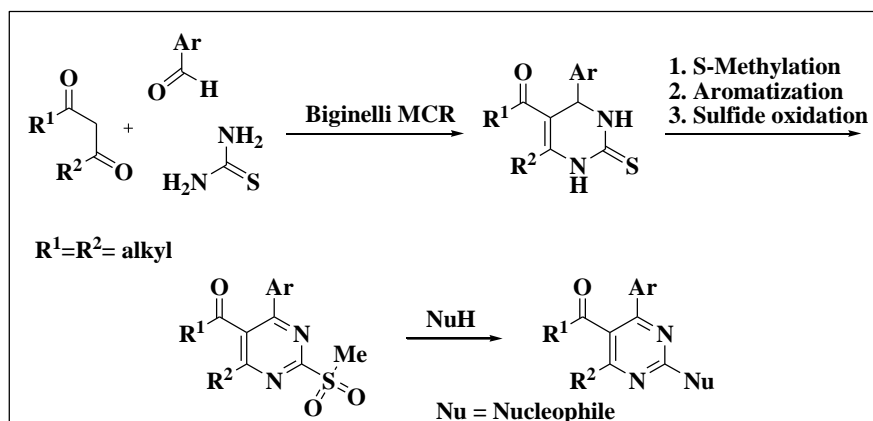
Yamamoto et al. [20] in 2005, introduced a mild, practical procedure for oxidative dehydrogenation of dihydropyrimidinones and most dihydropyrimidines with catalytic amounts of a Cu salt,  $\text{K}_2\text{CO}_3$ , and tert-butylhydroperoxide (TBHP) as a terminal oxidant in dichloromethane for 15-24 h (**Scheme 3A.5**). A mechanistic proposal involves coordination of the metal catalyst to NH moiety, followed by oxidative elimination of the resulting metal complex.



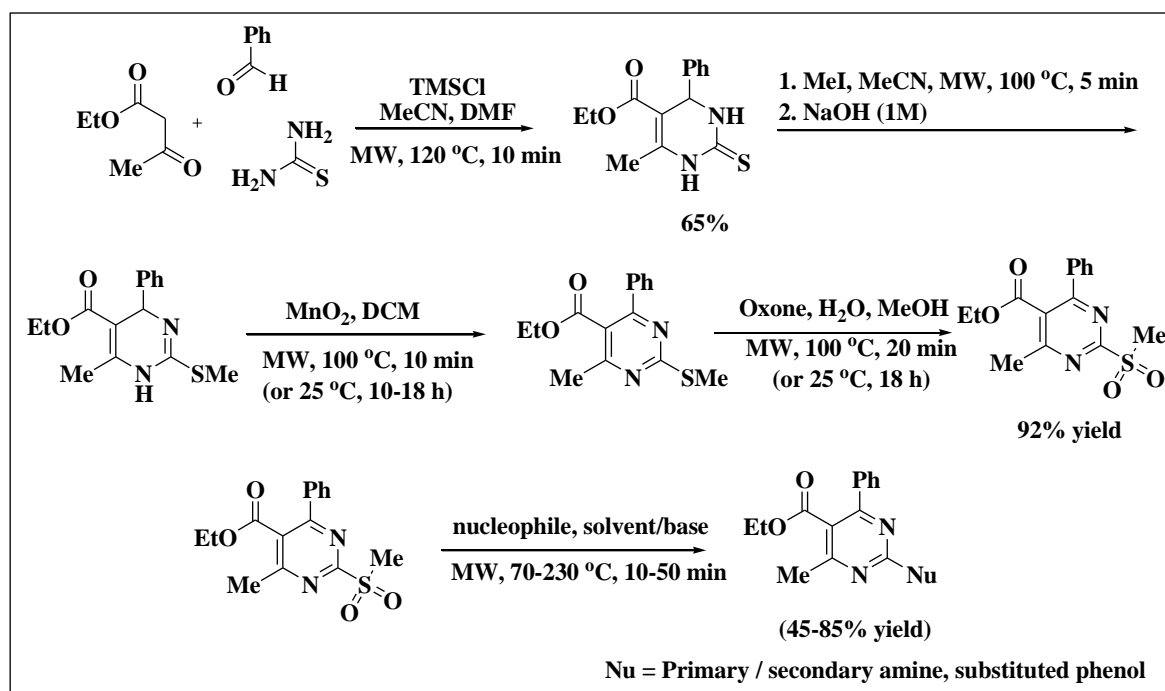
**Scheme 3A.5:** Oxidative dehydrogenation of dihydropyrimidinones

Matloobi et al. in 2007 [21] described an efficient and rapid microwave-assisted solution-phase method for the synthesis of 2-amino-4-arylpyrimidine-5-carboxylic acid derivatives involving a five-step linear conversion of Biginelli DHPMs via S-methylation, aromatization, sulfide oxidation and nucleophilic substitution (**Scheme 3A.6**). The initially formed dihydropyrimidine-2-thiones are converted to 2-methylthiodihydropyrimidines in presence of MeI. The products obtained from this step

oxidized first with manganese dioxide and then with oxone to provide 2-methylsulfonylpyrimidines which serve as excellent precursors for the generation of a variety of 2-substituted pyrimidines via displacement of the reactive sulfonyl group with nitrogen, oxygen, sulfur, and carbon nucleophiles. The oxidation steps required longer time at room temperature reaction for the model reaction in organic solvent like DCM and MeOH/water (**Scheme 3A.7**). They also utilized a modified protocol using a solid-phase method in the same report.



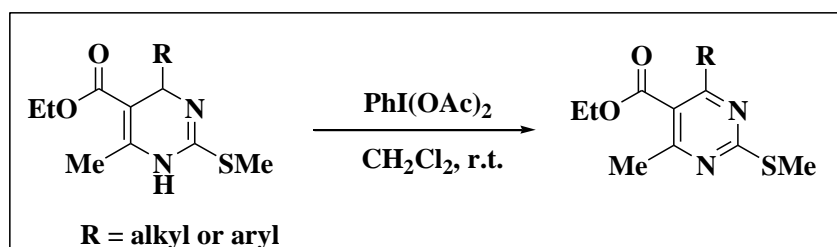
**Scheme 3A.6:** Four-step conversion of Biginelli DHPMs to 2-amino-4-arylpurines



**Scheme 3A.7:** Detail procedure for conversion of dihydropyrimidine-2-thiones to 2-substituted pyrimidines

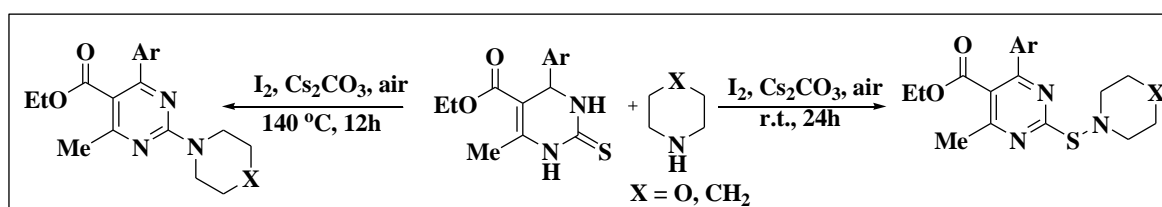
The oxidative dehydrogenation method was also successfully employed with 4-Alkyl or aryl-1,4-dihydropyrimidines by Karade et al. [22] using (diacetoxyido)benzene under mild reaction conditions to the corresponding pyrimidine

derivatives in good to excellent yields (63-81%) for 1 h reaction at room temperature in dichloromethane (**Scheme 3A.8**). The optimized conditions for the oxidative aromatization of 2-methylthio-1, 4-dihydropyrimidine requires four or five equivalents of  $\text{Mn}(\text{OAc})_3$  or  $\text{MnO}_2$  respectively under different reaction conditions [21, 23].



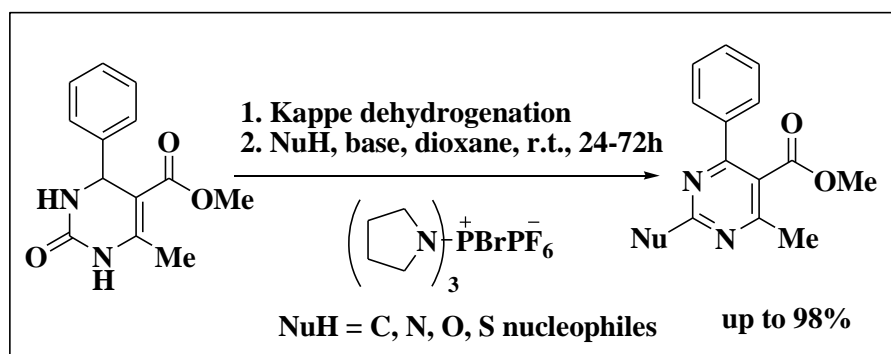
**Scheme 3A.8:** Dehydrogenation of 4-alkyl or aryl-1, 4-dihydropyrimidines to pyrimidine derivatives reported by Karade et al.

Wang et al. in 2013 reported a simple iodine mediated S-N or C-N cross-coupling and oxidative-aromatization of 3, 4-dihydropyrimidine-2(1H)-thiones with a secondary amine [4] (**Scheme 3A.9**). Remarkably the C-N coupled product was obtained via a desulfitative coupling-aromatization reaction in one-pot reaction.



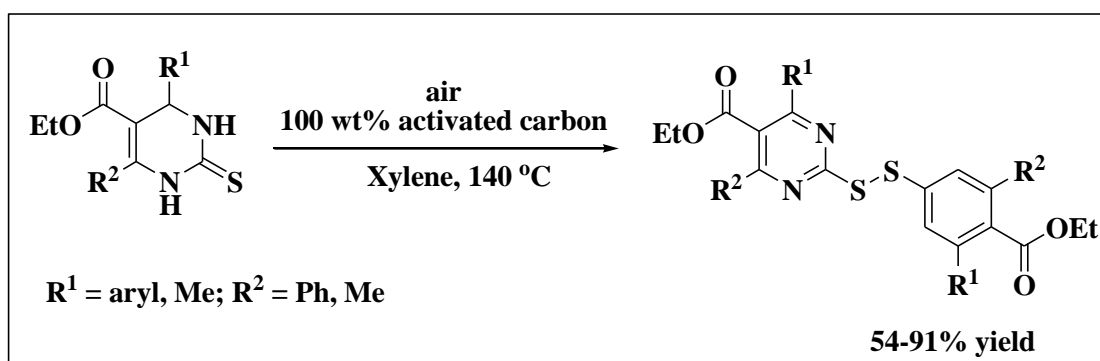
**Scheme 3A.9:** Conversion of 3, 4-dihydropyrimidine-2(1H)-thiones to pyrimidines as reported by Wang et al.

Kang et al. in 2005 [24] described an efficient two-step procedure to convert the Biginelli 3, 4-dihydropyrimidin-2(1H)-one to different multifunctionalized pyrimidines involving the Kappe dehydrogenation and a new mild PyBroP-mediated coupling with C, N, O, and S nucleophiles, which provides a readily accessible multifunctionalized pyrimidine template for diversity oriented synthesis at room temperature during 24-72 h reaction in 2<sup>nd</sup> step (**Scheme 3A.10**).



**Scheme 3A.10:** Conversion of Biginelli 3,4-dihydropyrimidin-2(1*H*)-one to different multifunctionalized pyrimidines

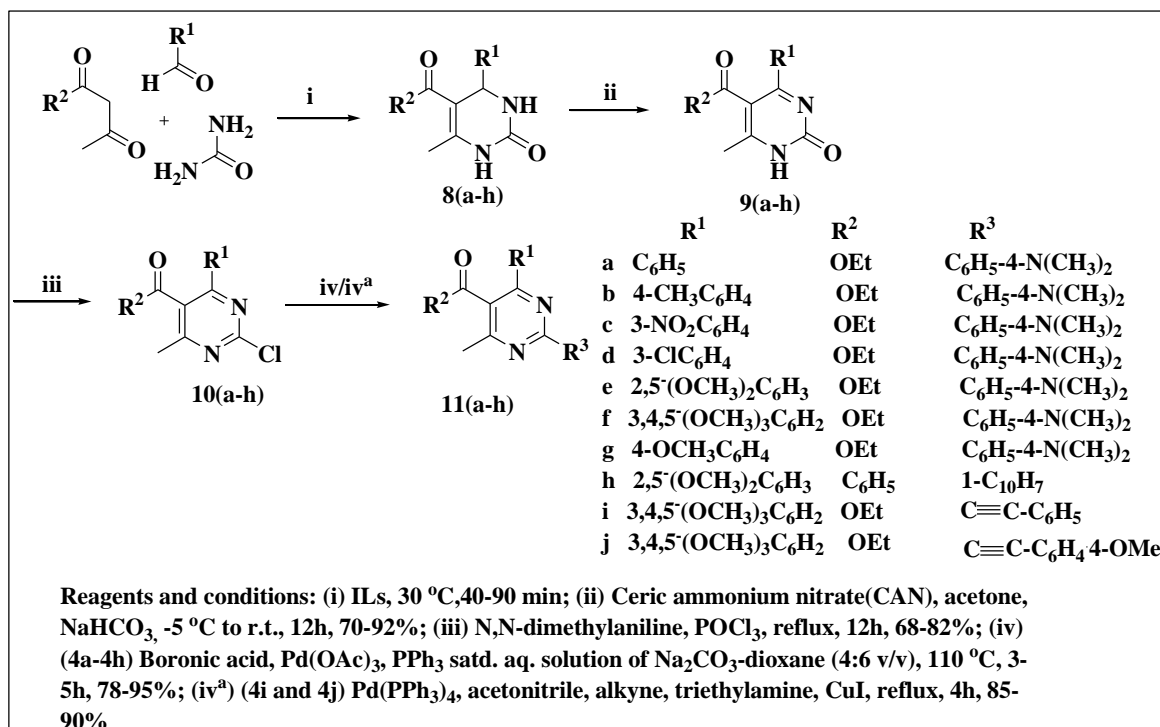
Hayashi et al. [25] developed an efficient oxidative transformation of 3,4-dihydropyrimidin-2(1*H*)-thiones to disulfide in the presence of activated carbon under an oxygen (or air) atmosphere during 36-67 h reaction time under reflux condition in xylene (**Scheme 3A.11**).



**Scheme 3A.11:** Oxidation of functionalized 3,4-dihydropyrimidin-2(1*H*)-thiones

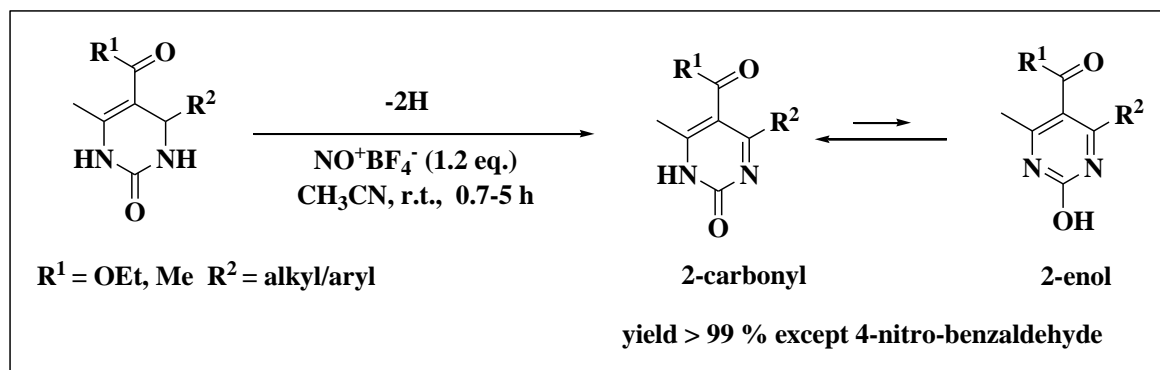
Gholap et al. [26] developed a four step protocol for synthesis of diversely substituted novel pyrimidines. A series of chlorinated pyrimidines were synthesized from easily available Biginelli 3, 4-dihydropyrimidin-2(1*H*)-ones via dehydrogenation, chlorination (**Scheme 3A.12**). The chlorinated pyrimidines were utilized to the conditions normally employed for palladium catalyzed C–C Suzuki/Sonogashira coupling reactions to obtain C- phenyl pyrimidines. They also found these molecules with excellent in vitro antifungal and antibacterial profiles.





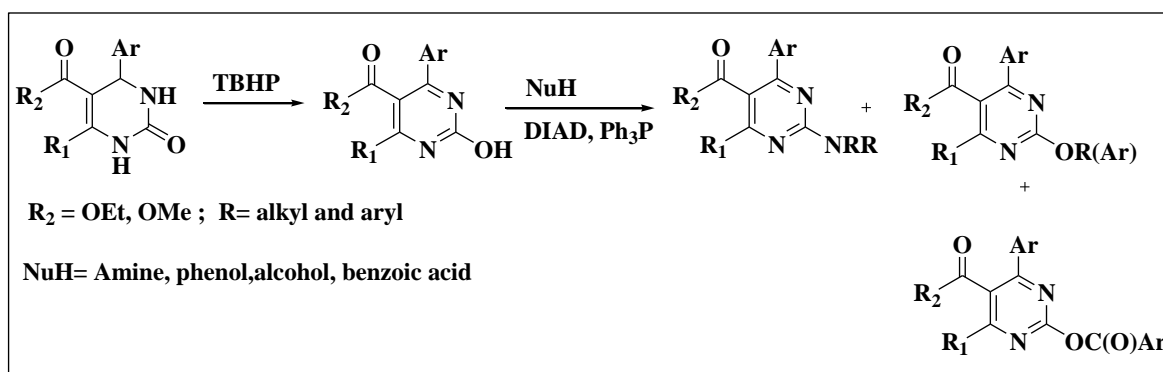
**Scheme 3A.12:** Preparation of diversely substituted novel pyrimidines reported by Gholap et al.

Liang et al. [27] oxidized 3, 4-dihydropyrimidin-2(1H)-ones (DHPMs) with 1.2 equiv. of nitrosonium tetrafluoroborate (NO<sup>+</sup>BF<sub>4</sub><sup>-</sup>) to pyrimidin-2(1H)-ones in acetonitrile at room temperature in high yields (**Scheme 3A.13**).



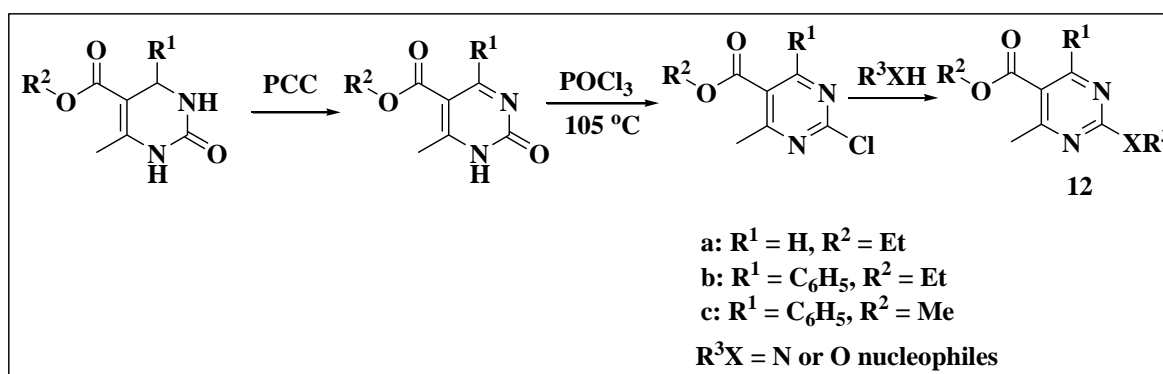
**Scheme 3A.13:** Oxidation 3, 4-dihydropyrimidin-2(1H)-ones (DHPMs) to pyrimidin-2(1H)-ones

Wang et al. [28] converted Biginelli 3,4-dihydropyrimidin-2(1H)-one to various C2-multifunctionalized pyrimidines via the dehydrogenation and Mitsunobu reaction using amines, alcohols, phenols and carboxylic acids as nucleophiles (**Scheme 3A.14**).



**Scheme 3A.14:** Preparation of C2-multifunctionalized pyrimidines

Singh et al. [29] developed a three step transformation of DHPMs to pyrimidines bearing amine substituents at C-2 position according to reaction **Scheme 3A.15**. The methodology has the potential for incorporation of tailor-made substituents at the C-2 position of DHPMs in a synthetically useful manner. The compounds were found to possess structure dependent cytostatic activity, these were not found to be efficient inhibitors of *Mycobacterium tuberculosis* nor did they inhibit a broad variety of DNA or RNA viruses in cell culture.



**Scheme 3A.15:** Synthesis of 2-substituted 5-carboxylate derivatives

Most of the reported methods are carried out in several steps at high temperature reaction with isolation of various reaction intermediates formed in different steps. Some of the steps require longer reaction time to produce good yield of products. In this context, we decided to design a simpler and environmentally benign efficient one pot sequential multistep route for conversion of Biginelli DHPMs to 2-aminopyrimidine derivatives pyrimidines under mild reaction conditions.

---

**References**

1. Lagoja, I. M. Pyrimidine as constituent of natural biologically active compounds. *Chemistry & Biodiversity*, 2(1):1-50, 2005.
2. Kappe, C. O. Biologically active dihydropyrimidones of the Biginelli-type-a literature survey. *European Journal of Medicinal Chemistry*, 35(12):1043-1052, 2000.
3. Chiang, A. N., Valderramos, J. C., Balachandran, R., Chovatiya, R. J., Mead, B. P., Schneider, C., Bell, S. L., Klein, M. G., Huryn, D. M., Chen, X. S., and Day, B. W. Select pyrimidinones inhibit the propagation of the malarial parasite, *Plasmodium falciparum*. *Bioorganic & Medicinal Chemistry*, 17(4):1527-1533, 2009.
4. Quan, Z. J., Lv, Y., Wang, Z. J., Zhang, Z., Da, Y. X., and Wang, X. C. Molecular iodine-mediated S–N and C–N cross-coupling and oxidative aromatization of 3, 4-dihydropyrimidin-2 (1H)-thiones with secondary amines. *Tetrahedron Letters*, 54(14):1884-1887, 2013.
5. Kappe, C. O. and Roschger, P. Synthesis and reactions of “Biginelli-compounds”. Part I. *Journal of Heterocyclic Chemistry*, 26(1):55-64, 1989.
6. Watanabe, M., Koike, H., Ishiba, T., Okada, T., Seo, S., and Hirai, K. Synthesis and biological activity of methanesulfonamide pyrimidine-and N-methanesulfonyl pyrrole-substituted 3, 5-dihydroxy-6-heptenoates, a novel series of HMG-CoA reductase inhibitors. *Bioorganic & Medicinal Chemistry*, 5(2):437-444, 1997.
7. Kappe, C. O. 100 years of the Biginelli dihydropyrimidine synthesis. *Tetrahedron*, 49(32):6937-6963, 1993.
8. Eynde, J. J. V., Audiart, N., Canonne, V., Michel, S., Van Haverbeke, Y., and Kappe, C. O. Synthesis and aromatization of dihydro-pyrimidines structurally related to calcium channel modulators of the nifedipine-type. *Heterocycles*, 10(45):1967-1978, 1997.
9. Puchala, A., Belaj, F., Kappe, C. O. and Bergman, J. On the reaction of 3, 4-dihydropyrimidones with nitric acid. Preparation and X-ray structure analysis of a stable nitrolic acid. *Journal of Heterocyclic Chemistry*, 38(6):1345-1352, 2001.

10. Loev, B. and Snader, K. M. The Hantzsch reaction. I. Oxidative dealkylation of certain dihydropyridines. *The Journal of Organic Chemistry*, 30(6):1914-1916, 1965.
11. Eynde, J. J. V., Mayence, A., and Maquestiau, A. A novel application of the oxidizing properties of pyridinium chlorochromate: aromatization of Hantzsch 1, 4-dihydropyridines. *Tetrahedron*, 48(3):463-468, 1992.
12. Pfister, J. R. Rapid, high-yield oxidation of Hantzsch-type 1, 4-dihydropyridines with ceric ammonium nitrate. *Synthesis*, 1990(08):689-690, 1990.
13. Eynde, J. J. V., Delfosse, F., Mayence, A., and Van Haverbeke, Y. Old reagents, new results: Aromatization of Hantzsch 1, 4-dihydropyridines with manganese dioxide and 2, 3-dichloro-5, 6-dicyano-1, 4-benzoquinone. *Tetrahedron*, 51(23):6511-6516, 1995.
14. Hankovszky, O. H., Sár, C. P., Hideg, K., and Jerkovich, G. Synthesis of spin-labelled 1, 4-dihydropyridines and pyridines. *Synthesis*, 1991(01):91-97, 1991.
15. Fatiadi, A. J. Active manganese dioxide oxidation in organic chemistry-part I. *Synthesis*, 1976(02):65-104, 1976.
16. Fatiadi, A. J. Active manganese dioxide oxidation in organic chemistry-part II. *Synthesis*, 1976(03):133-167, 1976.
17. Eynde, J. J. V., D'Orazio, R., and Van Haverbeke, Y. Potassium permanganate, a versatile reagent for the aromatization of Hantzsch 1, 4-dihydropyridines. *Tetrahedron*, 50(8):2479-2484, 1994.
18. Walker, D. and Hiebert, J. D. 2, 3-Dichloro-5, 6-dicyanobenzoquinone and its reactions. *Chemical Reviews*, 67(2):153-195, 1967.
19. Shanmugam, P. and Perumal, P. T. Regioselective dehydrogenation of 3, 4-dihydropyrimidin-2 (1H)-ones mediated by ceric ammonium nitrate. *Tetrahedron*, 62(41):9726-9734, 2006.
20. Yamamoto, K., Chen, Y. G., and Buono, F. G. Oxidative dehydrogenation of dihydropyrimidinones and dihydropyrimidines. *Organic Letters*, 7(21):4673-4676, 2005.
21. Matloobi, M. and Kappe, C. O. Microwave-assisted solution-and solid-phase synthesis of 2-amino-4-arylpyrimidine derivatives. *Journal of Combinatorial Chemistry*, 9(2):275-284, 2007.

22. Karade, N. N., Gampawar, S. V., Tale, N. P., and Kedar, S. B. Mild and efficient oxidative aromatization of 4-substituted-1, 4-dihydropyrimidines using (diacetoxyiodo) benzene. *Journal of Heterocyclic Chemistry*, 47(3):740-744, 2010.
23. Akhtar, M. S., Seth, M., and Bhaduri, A. P. Synthesis of 2, 3-dihydro-5H-thiazolo (3, 2-a) pyrimidines and tetra substituted dihydropyrimidines and tetra substituted dihydropyrimidine derivatives as possible anthelmintic agents. *Indian Journal of Chemistry B*, 26:556-561, 1987.
24. Kang, F. A., Kodah, J., Guan, Q., Li, X., and Murray, W. V. Efficient conversion of Biginelli 3, 4-dihydropyrimidin-2 (1 H)-one to pyrimidines via PyBroP-mediated coupling. *The Journal of Organic Chemistry*, 70(5):1957-1960, 2005.
25. Hayashi, M., Okunaga, K. I., Nishida, S., Kawamura, K., and Eda, K. Oxidative transformation of thiols to disulfides promoted by activated carbon-air system. *Tetrahedron Letters*, 51(51):6734-6736, 2010.
26. Gholap, A. R., Toti, K. S., Shirazi, F., Deshpande, M. V., and Srinivasan, K. V. Efficient synthesis of antifungal pyrimidines via palladium catalyzed Suzuki/Sonogashira cross-coupling reaction from Biginelli 3, 4-dihydropyrimidin-2 (1H)-ones. *Tetrahedron*, 64(44):10214-10223, 2008.
27. Liang, R. R., Wu, G. L., Wu, W. T., and Wu, L. M. Oxidation of 3, 4-dihydropyrimidin-2 (1H)-ones with nitrosonium (NO<sup>+</sup>). *Chinese Chemical Letters*, 20(10):1183-1186, 2009.
28. Wang, X. C., Yang, G. J., Jia, X. D., Zhang, Z., Da, Y. X., and Quan, Z. J. Synthesis of C2-functionalized pyrimidines from 3, 4-dihydropyrimidin-2 (1H)-ones by the Mitsunobu coupling reaction. *Tetrahedron*, 67(18):3267-3272, 2011.
29. Singh, K., Singh, K., Wan, B., Franzblau, S., Chibale, K., and Balzarini, J. Facile transformation of Biginelli pyrimidin-2 (1H)-ones to pyrimidines. In vitro evaluation as inhibitors of Mycobacterium tuberculosis and modulators of cytostatic activity. *European Journal of Medicinal Chemistry*, 46(6):2290-2294, 2011.

## ***Chapter 3B***

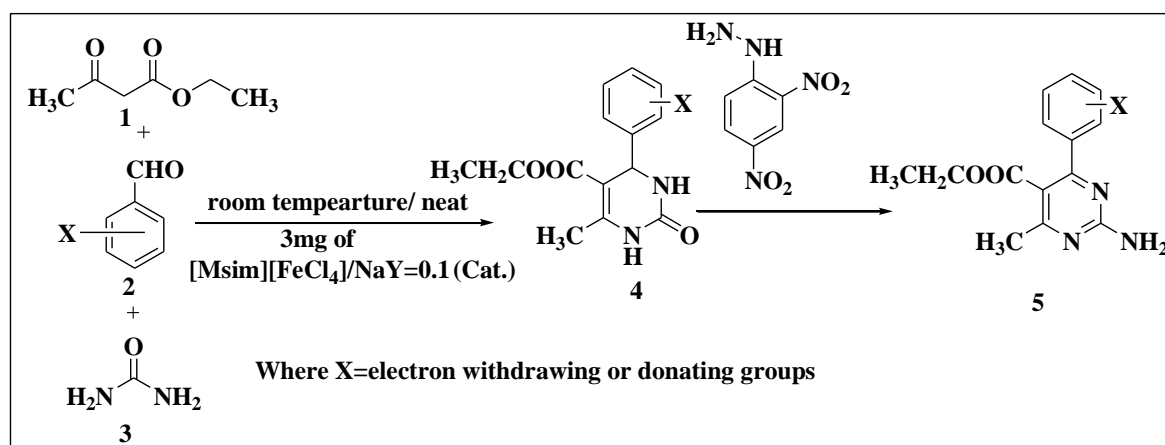
**Development of heterogenized hybrid catalyst of 1-sulfonic acid-3-methyl imidazolium ferric chloride over NaY zeolite and their utilization in one-pot synthesis of 2-amino-4-arylpyrimidine derivatives: A viable approach**

**Published with small modification**

**Gogoi, P., Dutta, A.K., Saikia, S., and Borah, R.** Heterogenized hybrid catalyst of 1-sulfonic acid-3-methyl imidazolium ferric chloride over NaY zeolite for one-pot synthesis of 2-amino-4-arylpyrimidine derivatives: A viable approach. *Applied Catalysis A: General*, 523:321-331, 2016.

### 3B.1. Results and discussion

In this section, a new series of acidic hybrid material of NaY zeolite were synthesized by modifying the zeolite surface with an acidic ionic salt: 1-sulfonic acid-3-methyl imidazolium ferric chloride ( $[\text{Msim}][\text{FeCl}_4]$ ) via wet impregnation method. The NaY zeolite powder and  $[\text{Msim}][\text{FeCl}_4]$  were mixed in six different weight/weight ratios (such as 0.03, 0.05, 0.1, 0.2, 0.5 & 1) using a few drops of EtOAc. These composites were fully characterized by Powder XRD, FT-IR, Raman, TGA, SEM-EDX, TEM, BET, ICP-OES and Hammett acid strength measurement methods. After observing their structural changes, thermal stability and Hammett acidity, the catalytic activity of the composites were examined for the novel one-pot consecutive transformation of Biginelli 3, 4-dihydropyrimidin-2-(*1H*)-ones to 2-amino-4-arylpyrimidines (**Scheme 3B.1**).



**Scheme 3B.1:** General route for synthesis of 2-amino-4-arylpyrimidine derivatives (**5**)

#### *Powder XRD analysis*

The powder XRD patterns of NaY and modified zeolite composites (**Fig. 3B.1**) support the preservation of zeolite framework up to the w/w ratio of 0.2. Above that, complete destruction of the framework occurs which can be attributed for acid induced dealumination of Y-zeolite at 150 °C to maximum amount of extra framework aluminium species (EFAI) in presence of higher loaded (0.5 & 1)  $-\text{SO}_3\text{H}$  containing  $[\text{Msim}][\text{FeCl}_4]$  ionic solid [1-4]. A small peak was observed at  $2\theta = 45.13^\circ$  for all composites which becomes prominent for **e** (0.2), **f** (0.5) and **g** (1) composites. Partial ionic interaction between Fe species and zeolite framework could also occur during impregnation and was found to be more effective beyond  $[\text{Msim}][\text{FeCl}_4]/\text{NaY}=0.2$  ratio. The extra peak centered at  $2\theta=45.13^\circ$  matches well with the XRD database of  $\text{FeCl}_3$  (JCPDS card no. 770999) and represents the attachment of  $[\text{FeCl}_4]^-$  species with the

zeolite surface. On modification, the crystallinity of the zeolite particles decreases and it has a direct correlation with loading percentages. This implies that partial dealumination transforms a portion of crystalline zeolite into amorphous state along with preservation of significant fraction of crystallinity in the **Fig. 3B.1** up to 0.2 (e) loading of [Msim][FeCl<sub>4</sub>] salt [5].

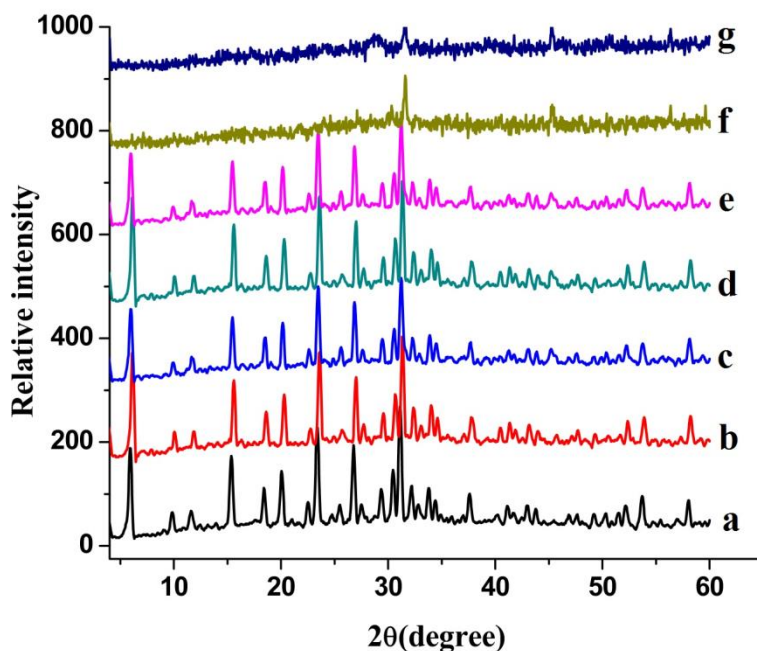


**Fig. 3B.1:** Powder XRD spectrum of the parent and modified NaY zeolite sample; **a:**NaY, **b:**[Msim][FeCl<sub>4</sub>]/NaY=0.03, **c:**[Msim][FeCl<sub>4</sub>]/NaY=0.05, **d:**[Msim][FeCl<sub>4</sub>]/NaY=0.1, **e:**[Msim][FeCl<sub>4</sub>]/NaY=0.2, **f:**[Msim][FeCl<sub>4</sub>]/NaY=0.5, **g:**[Msim][FeCl<sub>4</sub>]/NaY=1

The relative crystallinity difference between modified samples and the parent zeolite were compared by taking four high intensity peaks at  $2\theta = 15.3^\circ$ ,  $23.48^\circ$ ,  $26.85^\circ$  and  $31.05^\circ$ . An informative **Table 3B.1** is generated and it is illustrated in **Fig. 3B.2**.

**Table 3B.1:** Comparison of the percent crystallinity of modified samples with the parent zeolite

2θ values	Relative intensity				
	NaY	[Msim][FeCl <sub>4</sub> ]/NaY=0.03	[Msim][FeCl <sub>4</sub> ]/NaY= 0.05	[Msim][FeCl <sub>4</sub> ]/NaY= 0.1	[Msim][FeCl <sub>4</sub> ]/NaY= 0.2
15.3	100	78.69	72.5	67.8	39.38



23.48	100	97.32	78.74	77	58.06
26.85	100	99.63	87.77	74.4	56.21
31.05	100	73.08	69.47	62.72	46.20

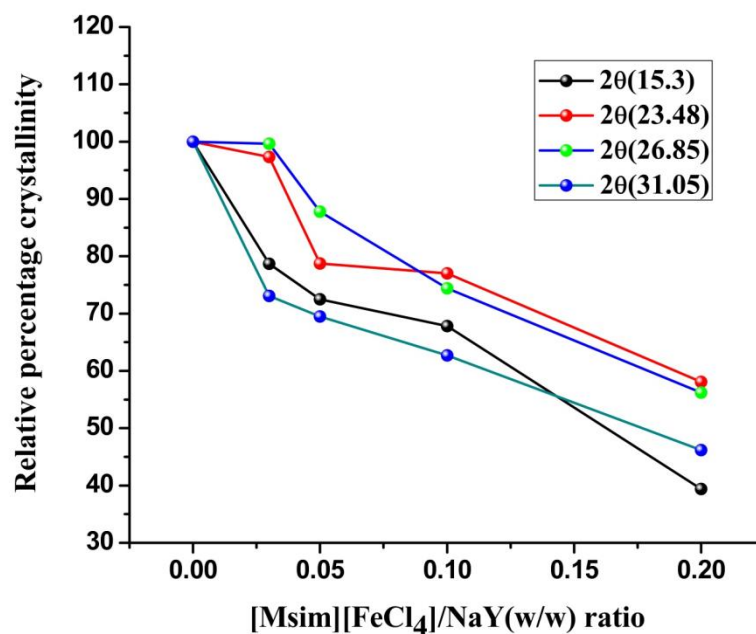


**Fig. 3B.2:** Comparison of the percent crystallinity of modified samples with the parent zeolite

### *FT-IR analysis*

FT-IR spectra of the parent and the modified samples were recorded and represented in **Fig. 3B.3** in the region  $400\text{-}1800\text{ cm}^{-1}$ . The 0.2(e) loaded sample shows optimum dealumination state, without a significant change of basic vibrational frequencies of NaY zeolite like powder X-ray analysis (**Fig. 3B.1**) [6]. The sharp band in the region of  $1638\text{-}1642\text{ cm}^{-1}$  for all composites can be considered for bending vibration of water molecules attached to the zeolite structure including  $\text{-C=N-}$  stretching vibration of imidazolium cation of ionic salt [7]. The O-H stretching vibration at  $3459\text{ cm}^{-1}$  for parent zeolite shifts its position to  $3441\text{ cm}^{-1}$  with an intense peak for the composite  $[\text{Msim}][\text{FeCl}_4]/\text{NaY} = 1(\text{g})$  and this represents the existence of strong hydrogen bonding within the composite involving hydroxyl group [8].

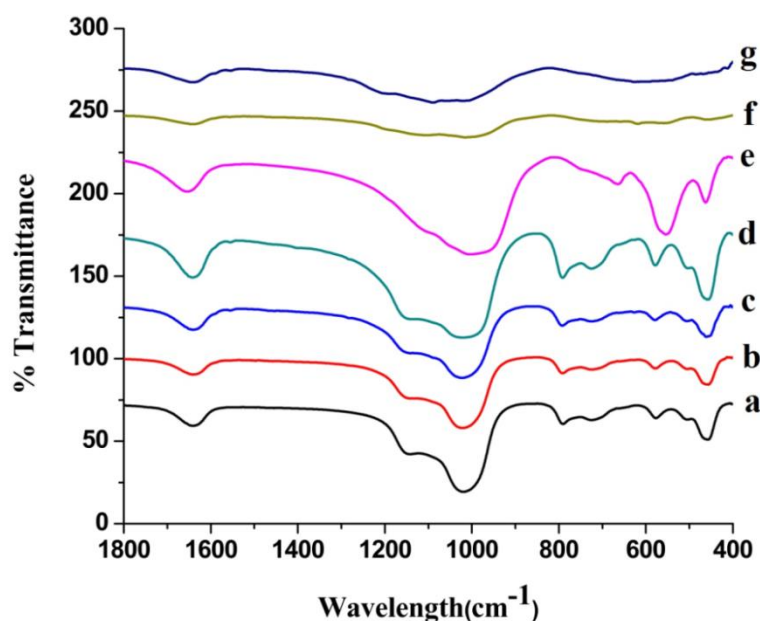


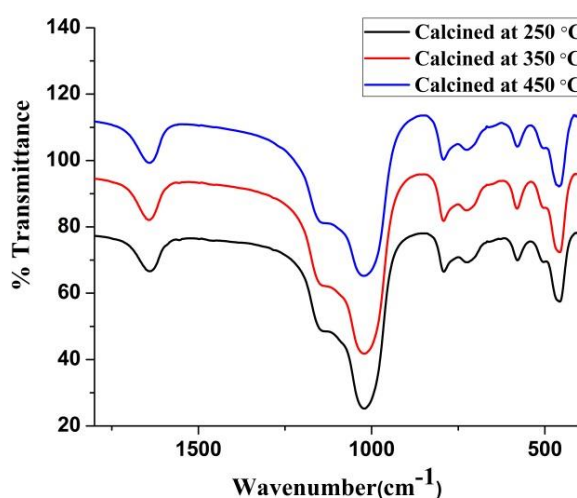
**Fig. 3B.3:** FT-IR spectra of the parent as well as modified NaY zeolite samples, where **a:**NaY, **b:**[Msim][FeCl<sub>4</sub>]/NaY=0.03, **c:**[Msim][FeCl<sub>4</sub>]/NaY=0.05, **d:**[Msim][FeCl<sub>4</sub>]/NaY=0.1, **e:**[Msim][FeCl<sub>4</sub>]/NaY=0.2, **f:**[Msim][FeCl<sub>4</sub>]/NaY=0.5, **g:**[Msim][FeCl<sub>4</sub>]/NaY=1

The framework sensitive double-ring vibration peak at 577 cm<sup>-1</sup> of NaY observed around 578-579 cm<sup>-1</sup> for the composites of 0.03(**b**), 0.05(**c**), 0.1(**d**) and 0.2(**e**). The other characteristic frequencies of NaY zeolite, corresponding to bending, symmetrical and asymmetrical stretching vibrations of TO<sub>4</sub> (Si or Al) building units have been displayed at 455-458 cm<sup>-1</sup>, 721-793 cm<sup>-1</sup> and 1019-1143 cm<sup>-1</sup> for the above four composites [9]. The strong S-O symmetric and asymmetric stretching and bending vibrations of ionic salt at 1222 cm<sup>-1</sup>, 1075 cm<sup>-1</sup> and 618 cm<sup>-1</sup> are also overlapping with the above fundamental vibrations of TO<sub>4</sub> unit of NaY zeolite [7]. The characteristic absorption peaks of the composites almost disappeared for 0.5 (**f**) and 1 (**g**) [Msim][FeCl<sub>4</sub>]/NaY samples which can be accounted for destruction of the parent zeolite framework by rapid acid mediated dealumination process in these two samples to form large amount of non-framework Al species such as Al(OH)<sub>2</sub><sup>+</sup> or AlO<sup>+</sup> etc. [10, 11].

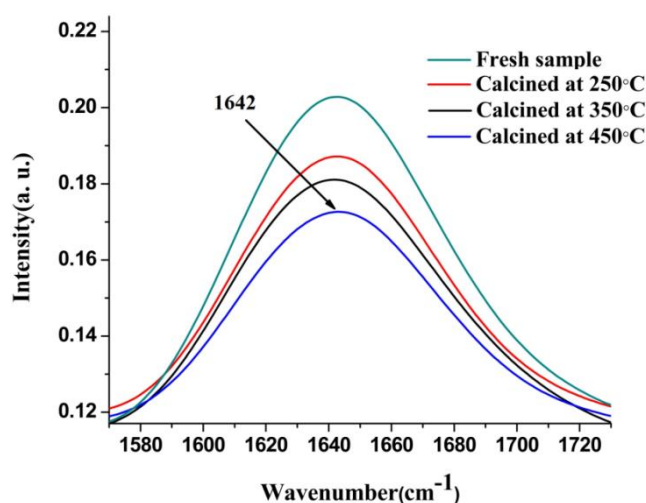
From the above discussion of IR studies, we can assume that the modified samples have some extra framework species of aluminosilicate and silica gel formed by partial or complete destruction of the parent framework during preparation of [Msim][FeCl<sub>4</sub>] loaded composites with NaY. Furthermore, the identical FT-IR spectra

of four composites (**b**, **c**, **d** & **e**) and NaY (**a**) represents insufficient dealumination inside the framework in presence of less amount of acidic salt [12].

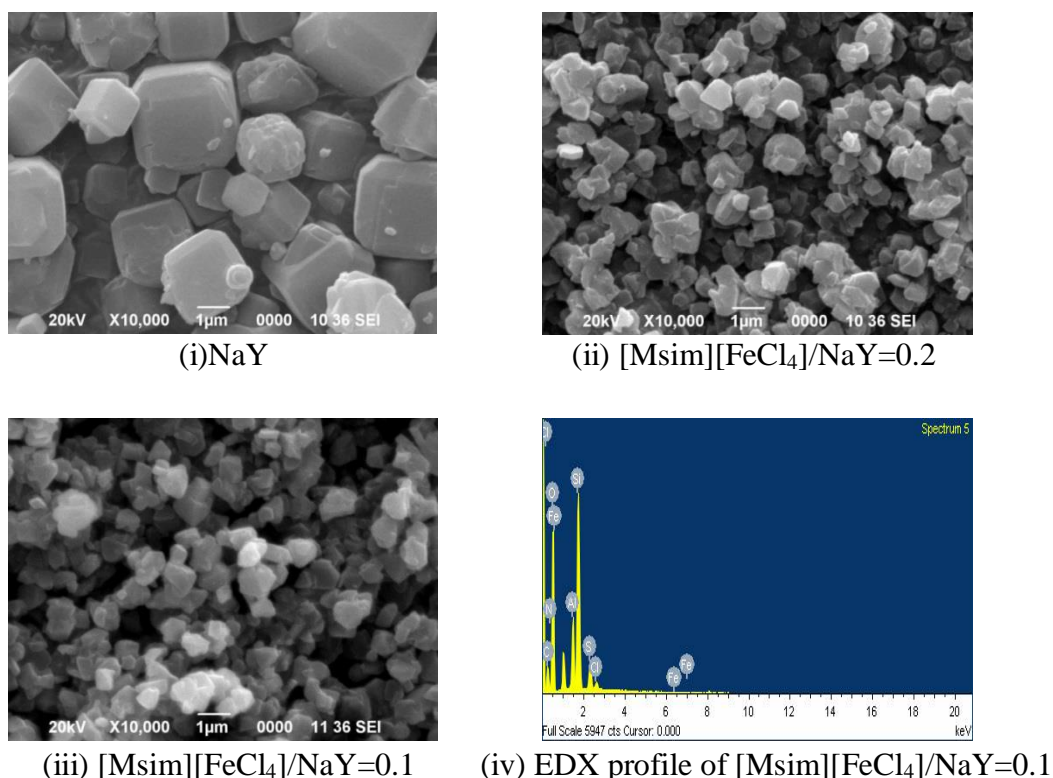
The recorded FT-IR spectra (**Fig. 3B.4**) of [Msim][FeCl<sub>4</sub>]/NaY=0.1 sample after calcination at 250 °C, 350 °C and 450 °C also witnessed complete intactness of characteristic bands of the fresh 0.1 (**d**) composite within 400-1800 cm<sup>-1</sup>. This observation supports the thermal stability of this composite with small portion of non-framework Al species in solid state [13, 14]. On the other hand, the intensity of O-H bending peaks gradually reduced at high temperature calcination which indicate the loss of some hydroxyls associated with the 1641 cm<sup>-1</sup> band up to 450 °C (**Fig. 3B.5**).



**Fig. 3B.4:** FT-IR spectra of the sample; [Msim][FeCl<sub>4</sub>]/NaY=0.1 calcined at 250 °C, 350 °C and 450 °C



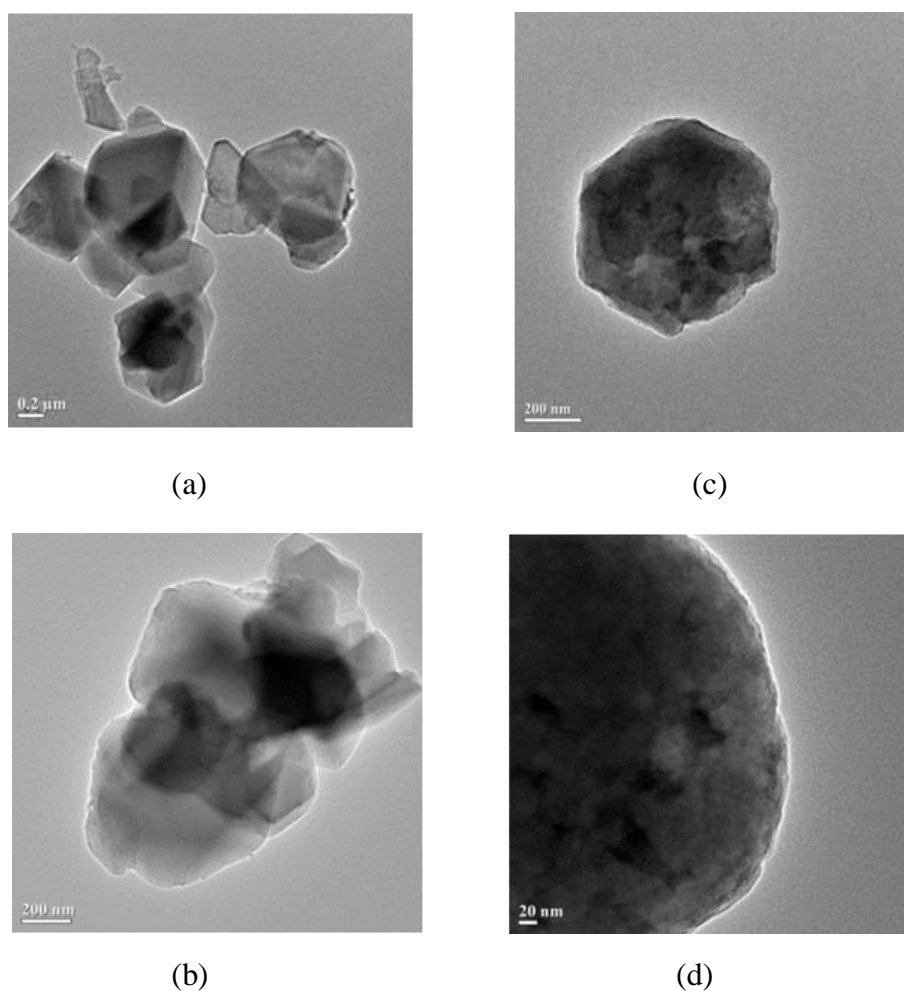
**Fig. 3B.5:** FT-IR spectra of bending vibrations of H<sub>2</sub>O molecules for 0.1(**d**) (Fresh & calcined at different temperatures)

*SEM-EDX analysis*

**Fig. 3B.6:** SEM images of (i)NaY, (ii)[Msim][FeCl<sub>4</sub>]/NaY=0.2, (iii)[Msim][FeCl<sub>4</sub>]/NaY=0.1, (iv) EDX profile for [Msim][FeCl<sub>4</sub>]/NaY=0.1 composite

**Fig. 3B.6** displays the SEM images of NaY zeolite, 0.1 (d) and 0.2 (e) [Msim][FeCl<sub>4</sub>]/NaY composites. Both the size and uniformity of the particles decrease on modification. Originally the parent NaY zeolite has cube like large particle structure. The change in surface morphology for the loaded materials depicts the anchoring of ionic solid on the surface of zeolite as smaller size cube type particles. They form more aggregation in case of w/w ratio of 0.2 than 0.1. This may convert the surface of [Msim][FeCl<sub>4</sub>]/NaY=0.2 composite to non-uniform in nature and decreases the number of acidic sites for catalytic performance.

The EDX spectra of the [Msim][FeCl<sub>4</sub>]/NaY=0.1 composite confirmed the presence of constituent elements of the ionic solid along with the zeolite.

*TEM analysis*

**Fig. 3B.7:** TEM images of [Msim][FeCl<sub>4</sub>]/NaY=0.1 composite

The TEM imaging was carried out for the [Msim][FeCl<sub>4</sub>]/NaY=0.1 composite zeolite at high resolution (**Fig. 3B.7**). These images proved that in the composite the crystallinity of basic NaY zeolite was preserved as observed in the PXRD pattern in **Fig. 3B.1**. No significant damages were detected on the hexagonal structure of NaY zeolite [15]. The TEM images also supported the accumulation of [Msim][FeCl<sub>4</sub>] salt as clusters on the external surface of zeolite in (c) and (d) similar to the SEM images (**Fig. 3B.6**).

*BET analysis***Table 3B.2: Textural properties of NaY and the composites**

Entry	Sample name	Surface area (m <sup>2</sup> /g)	Pore Volume (cm <sup>3</sup> /g)
1	NaY	900	0.32
2	[Msim][FeCl <sub>4</sub> ]/NaY=0.03	9	0.01
3	[Msim][FeCl <sub>4</sub> ]/NaY=0.05	16	0.01
4	[Msim][FeCl <sub>4</sub> ]/NaY=0.1	30	0.05
5	[Msim][FeCl <sub>4</sub> ]/NaY=0.2	38	0.03

**Table 3B.2** shows the BET surface area and pore volumes of NaY and four [Msim][FeCl<sub>4</sub>]/NaY composites. The composites displayed abrupt decrease of surface area as compared to NaY. This may be attributed to mostly non-porous coverage of zeolite surface by the ionic solid and can lead to restricted access to the zeolite pores for adsorption of N<sub>2</sub> gas. Interestingly, we also observed opposite trend for gradual increase of surface area and pore volume with increase in the percentage loading (entry 2-5, **Table 3B.2**). This trend can be supported by the phenomenon of more clustering of ionic solid on the zeolite surface as the loading increases, which was also further confirmed from SEM photograph (**Fig. 3B.6**). Such types of clusters formation indicate the non-porous coverage of zeolite surface through deposition of more ionic solids. It may create some porous host points into which the N<sub>2</sub> gas prefer to adsorb and thus it was reflected as increasing surface area in BET analysis in **Table 3B.2** against increase in the loading of ionic solid [16].

*Thermo gravimetric (TGA) analysis*

Thermo gravimetric analysis was conducted to compare the overall thermal stability of NaY, [Msim][FeCl<sub>4</sub>] and various composites of [Msim][FeCl<sub>4</sub>]/NaY (**Fig. 3B.8**). The small weight loss steps of NaY(**a**) and the composite materials 0.03(**b**) and 0.1(**d**) around 200 °C can be assigned to elimination of physisorbed or bound water attached to Na<sup>+</sup> of the parent framework (or hydrated cation for the modified samples) [17]. The amount of such water is more for the NaY (**a**) framework. For (**b**) and (**d**) samples, the number of Al content slightly decreases through partial exchange of proton

with  $\text{Na}^+$  which converts only a small fraction of the crystalline structure into non-framework Al species due to lower percentage of  $-\text{SO}_3\text{H}$  functionalized  $[\text{Msim}][\text{FeCl}_4]$  salt. It was found in some observations that appearance of EFAl brings a stabilizing effect to the modified zeolite framework by healing of Al defects with migrating  $\text{H}_4\text{SiO}_4$  molecules [18].

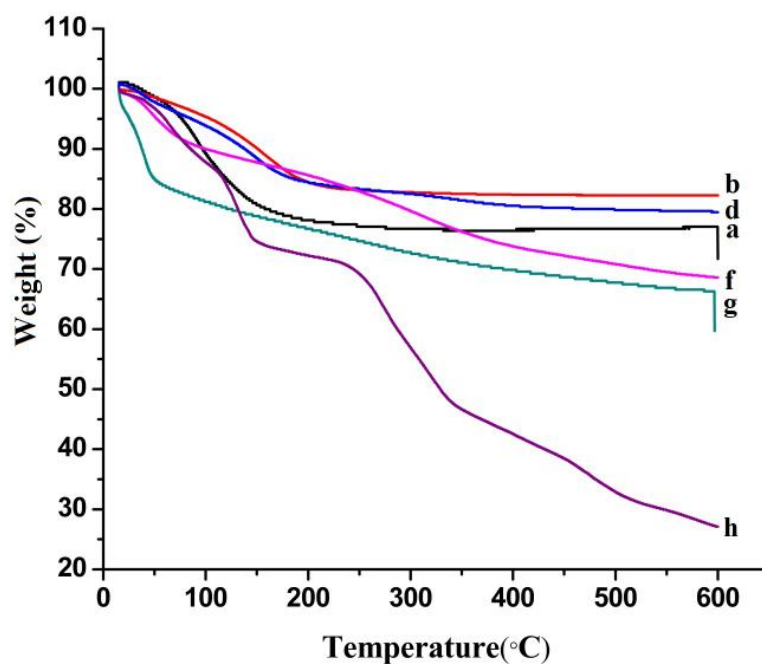


**Fig. 3B.8:** TGA profiles of parent zeolite and modified samples: (a) NaY; (b)  $[\text{Msim}][\text{FeCl}_4]/\text{NaY}=0.03$ ; (d)  $[\text{Msim}][\text{FeCl}_4]/\text{NaY}=0.1$ ; (f)  $[\text{Msim}][\text{FeCl}_4]/\text{NaY}=0.5$ ; (g)  $[\text{Msim}][\text{FeCl}_4]/\text{NaY}=1$ ; (h)  $[\text{Msim}][\text{FeCl}_4]$

Therefore, as compared to the parent zeolite, the modified samples (**b** & **d**) display smaller weight loss up to 200 °C. The moderate release of water molecule for 0.1 (**d**) composite with partial change of the basic  $\text{TO}_4$  frequencies (**Fig. 3B.3**) can also be evidenced from the comparative O-H bending vibration peak intensity observation at high temperature calcinations (**Fig. 3B.5**). Above 200 °C no significant weight loss was observed for these two samples 0.03 (**b**) and 0.1 (**d**) which can be speculated for probable ionic interaction of  $\text{FeCl}_4^-$  anion complex of  $\text{Na}^+$  exchanged ionic salt with partial Lewis acidic sites of the extra framework species such as  $\text{Al}^+(\text{OH})_2$ . As the loading of ionic solid increases from 0.5 (**f**) to 1 (**g**), the weight loss below 100 °C becomes rapid (approximately 15%) for the composite 1(**g**). At the same time, as evident from PXRD and FT-IR patterns, this composite witnessed the highest dealuminated state, so we cannot exclude the possibility of water loss below 100 °C



both from the hydrated cations and dehydroxylation of Al defects consisting of four silanols (Si-OH) [19]. The loss of water at 50 °C for the above sample (**g**) was further confirmed from the sudden drop of peak intensity for O-H stretching vibration around  $3441\text{ cm}^{-1}$  with two calcined samples at 50 °C and 100 °C (**Fig. 3B.9**). The two onset decomposition points for [Msim][FeCl<sub>4</sub>] ionic solid at 115-150 °C are enhanced to 170 °C in case of (**b**) and (**d**) and it raised to 200 °C for (**f**). The composite (**f**) witnessed gradual weight loss from 200 °C to 600 °C. A weight loss correlation table (**Table 3B.3**) for the hybrid catalysts was constructed.

**Table 3B.3:** Weight loss correlation with loading from TGA graph

Sample code name	w/w loading	Temperature(°C)	Weight loss (%)
<b>b</b>	0.03	200	15.9
<b>d</b>	0.1	-do-	15.6
<b>f</b>	0.5	-do-	13.3
<b>g</b>	1	-do-	14.4

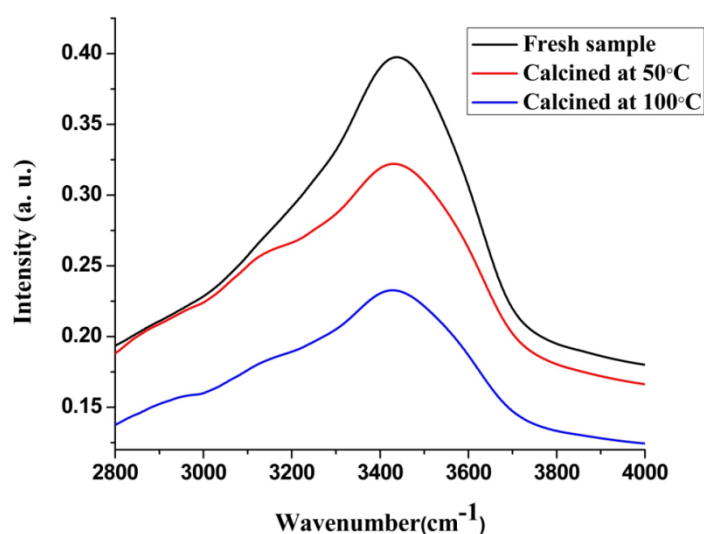


**Fig. 3B.9:** FT-IR spectra of OH stretching frequencies for 1(g) (Fresh & calcined at different temperatures)



*Raman analysis*

The Raman spectra for NaY and three composites are presented in **Fig. 3B.10**. The most intense peak for NaY zeolite was detected at  $500\text{ cm}^{-1}$  and is characteristics of the T-O-T bending vibration where T denotes Si or Al atoms of zeolite frameworks [20, 21]. For the composites, a broad shoulder at  $337\text{-}341\text{ cm}^{-1}$  was detected, which is exclusive proof of the presence of the ionic solid on the NaY zeolite surface [7]. The shoulder became prominent with increase in loading.

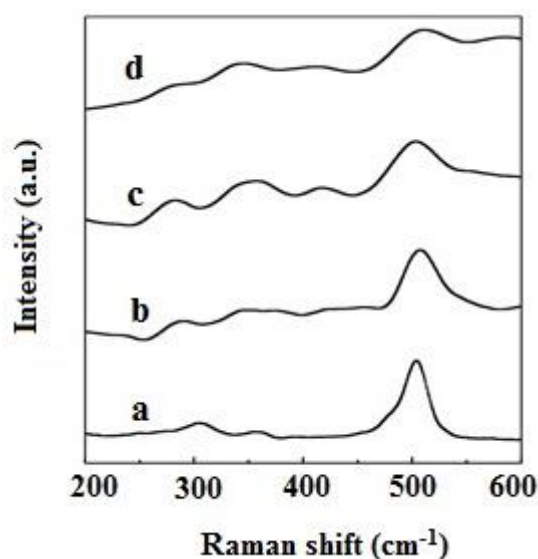


**Fig. 3B.10:** Comparison of the Raman spectra of (a)NaY; (b)[Msim][FeCl<sub>4</sub>]/NaY=0.03; (c)[Msim][FeCl<sub>4</sub>]/NaY=0.05; (d)[Msim][FeCl<sub>4</sub>]/NaY=0.2

*Acidity determination by Hammett plot*

The relative acidity of the composites was determined on an UV-Vis spectrophotometer with Hammett plots (**Fig. 3B.11a-11c**) using *p*-nitroaniline as the basic indicator [22] by following the same method as described in **Chapter 1C**. The procedure required mixing of equal concentration of 4-nitroaniline (5 mg/L,  $pK_a=0.99$ ) and catalyst (equal amounts of all) in ethanol solution. The indicator showed maximum absorbance at 378 nm in ethanol. The Hammett plot (**Fig. 3B.11a**) expressed the following decreasing acidity order of the four modified zeolite samples against their observed  $H^0$  values as (**Table 3B.4**): [Msim][FeCl<sub>4</sub>]/NaY=0.1(**d**)> [Msim][FeCl<sub>4</sub>]/NaY=0.05(**c**) [Msim][FeCl<sub>4</sub>]/NaY=0.03(**b**)>[Msim][FeCl<sub>4</sub>]/NaY=0.2(**e**). The formation of more clusters in case of (e) as supported by SEM analysis may block the active sites of the composites for interaction with the basic indicator and it leads to

decrease in the acidity of (e) as compared to (d). The powder XRD profile also indicates the destruction of the zeolite structure above w/w ratio of 0.2.

**Table 3B.4:** Calculation of the Hammett Function of the modified zeolite samples with equal concentration of composites and indicator

Entry	Sample name <sup>a</sup>	$A_{\max}$	[I]%	[IH]%	$H^0$
1.	Blank	2.493	100	0	-
2.	[Msim][FeCl <sub>4</sub> ]/NaY=0.03	1.256	50.4	49.6	0.997
3.	[Msim][FeCl <sub>4</sub> ]/NaY=0.05	1.244	49.9	50.1	0.988
4.	[Msim][FeCl <sub>4</sub> ]/NaY=0.1	1.209	48.49	51.51	0.964
5.	[Msim][FeCl <sub>4</sub> ]/NaY=0.2	1.311	52.59	47.40	1.035

<sup>a</sup>Indicator=*p*-nitroaniline

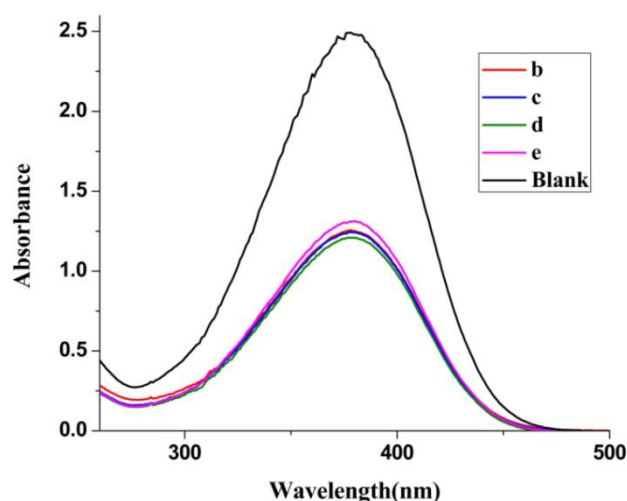


**Fig. 3B.11a** Hammett plots of the hybrid materials of zeolite samples by mixing equal concentration of indicator and composites: (b) [Msim][FeCl<sub>4</sub>]/NaY=0.03; (c) [Msim][FeCl<sub>4</sub>]/NaY=0.05; (d)[Msim][FeCl<sub>4</sub>]/NaY=0.1; (e) [Msim][FeCl<sub>4</sub>]/NaY=0.2.

To determine the effect of composite concentration on Hammett acidity, we also evaluated the acidity of the four composites in two different ratios (1:4 and 2:3) by altering the concentration of *p*-nitroaniline and composites respectively which produced two identical Hammett plots (**Fig. 3B.11b** and **Fig. 3B.11c**). Both the plots revealed the same acidity order (**Table 3B.5** & **Table 3B.6**) as observed from the Hammett plot (**Table 3B.4**) of equal concentration of the composites and indicator. With increasing

concentrations of the composites the unprotonated form of the basic indicator showed lower absorbance values.

**Table 3B.5:** Calculation of the Hammett Function of the modified zeolite samples with 1:4 ratio of the composites and indicator

Entry	Sample name <sup>a</sup>	$A_{\max}$	[I]%	[IH]%	$H^{\circ}$
1.	Blank	0.237	100	0	-
2.	[Msim][FeCl <sub>4</sub> ]/NaY=0.03	0.092	38.8	61.2	0.792
3.	[Msim][FeCl <sub>4</sub> ]/NaY=0.05	0.079	33.3	66.7	0.689
4.	[Msim][FeCl <sub>4</sub> ]/NaY=0.1	0.063	26.6	73.4	0.549
5.	[Msim][FeCl <sub>4</sub> ]/NaY=0.2	0.125	52.7	47.3	1.037

<sup>a</sup>Indicator=*p*-nitroaniline

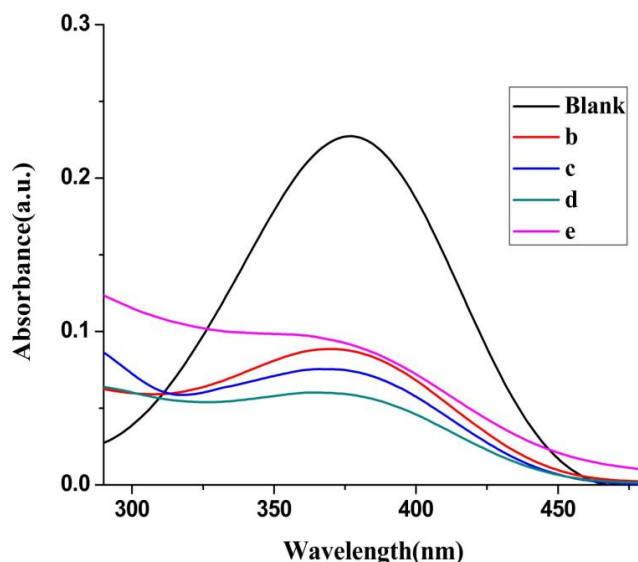


**Fig. 3B.11b:** Hammett plots of the hybrid materials of zeolite samples by mixing 1: 4 ratio of indicator and composites: (b) [Msim][FeCl<sub>4</sub>]/NaY=0.03; (c) [Msim][FeCl<sub>4</sub>]/NaY=0.05; (d)[Msim][FeCl<sub>4</sub>]/NaY=0.1; (e) [Msim][FeCl<sub>4</sub>]/NaY=0.2.

**Table 3B.6:** Calculation of the Hammett Function of the modified zeolite samples with 2:3 ratio of the composites and indicator

Entry	Sample name <sup>a</sup>	$A_{\max}$	[I]%	[IH]%	$H^{\circ}$
1.	Blank	0.237	100	0	-
2.	[Msim][FeCl <sub>4</sub> ]/NaY=0.03	0.110	46.4	53.6	0.927
3.	[Msim][FeCl <sub>4</sub> ]/NaY=0.05	0.106	44.7	55.3	0.897

4.	[Msim][FeCl <sub>4</sub> ]/NaY=0.1	0.103	43.5	56.5	0.876
5.	[Msim][FeCl <sub>4</sub> ]/NaY=0.2	0.155	65.4	34.6	1.267

<sup>a</sup>Indicator=*p*-itroaniline

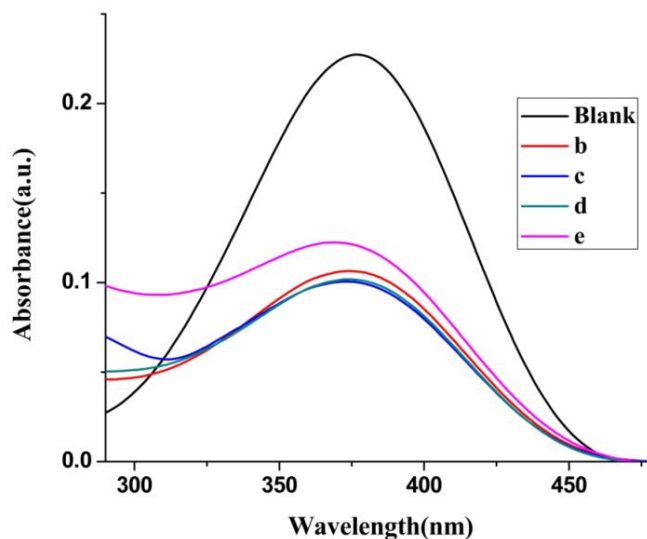


**Fig. 3B.11c:** Hammett plots of the hybrid materials of zeolite samples by mixing 2:3 ratio of indicator and composites: (b) [Msim][FeCl<sub>4</sub>]/NaY=0.03; (c) [Msim][FeCl<sub>4</sub>]/NaY=0.05; (d)[Msim][FeCl<sub>4</sub>]/NaY=0.1; (e) [Msim][FeCl<sub>4</sub>]/NaY=0.2

### *Evaluation of catalytic performance*

#### *Optimization of the reaction condition*

The acidic scale of the four composites with w/w ratio up to 0.2 has been determined through the Hammett plot. Due to small difference in acidity, we decided to test the catalytic activity of all of them. From the time frame required for completion of the reaction, the [Msim][FeCl<sub>4</sub>]/NaY=0.1 hybrid composite was chosen as the best acidic catalyst for the two-step one pot model synthesis of pyrimidine derivatives via in situ generation of Biginelli DHPMs from three component reaction of ethyl acetoacetate (1 mmol), benzaldehyde (1mmol) and urea (1.5 mmol) followed by reaction with 2,4-dinitrophenyl hydrazine (1 mmol) (**Table 3B.7**, entries 1-4). The catalytic activity of the composite was tested by varying the amount of catalyst (3/5/10/15 mg) at 60 °C in neat condition. Irrespective of the amount of the catalysts, the first step of reaction completed within 5-10 min without solvent at 60 °C as monitored by TLC plate (**Table 3B.7**, entries 3, 5-7). By conducting the reaction at room temperature, it has been observed

that only 3 mg of catalyst is sufficient to produce 3, 4-dihydropyrimidinone exclusively in 30 min (**Table 3B.7**, entry 8). However, no product formation was observed for the second step at room temperature. At 60 °C, 65-75% yield was observed for the second step in around 5-25 min duration using different amounts of the catalyst (3/5/10/15 mg) (**Table 3B.7**, entries 3, 5-7). Therefore, we decided to carry out the 2nd step at 80 °C and it gave improved result. Almost 87% yield was observed in 10 min (**Table 3B.7**, entry 8). We have also checked the utility of this catalytic system for industrial scale reactions by performing the same reaction on 20 mmol scale. We are pleased to report here that the composite was able to maintain its activity at that scale under the optimized conditions and has successfully completed the reaction within 10 minutes in 2nd step.

**Table 3B.7:** Optimization study for the one pot synthesis of pyrimidine derivatives

Entry	Catalyst	Amount of the catalyst(mg)	1st step	2nd step	% Yield <sup>a</sup> 5a
			Time(min)	Time(min)	
1.	[Msim][FeCl <sub>4</sub> ]/NaY=0.03	15	7	10	72
2.	[Msim][FeCl <sub>4</sub> ]/NaY=0.05	15	5	10	73
3.	[Msim][FeCl <sub>4</sub> ]/NaY=0.1	15	3	5	75
4.	[Msim][FeCl <sub>4</sub> ]/NaY=0.2	15	10	15	70
5.	[Msim][FeCl <sub>4</sub> ]/NaY=0.1	10	5	12	70
6.	-do-	5	10	20	68
7.	-do-	3	10	25	65
8.	-do-	3	30	10	87 <sup>b</sup>

<sup>a</sup>Reactions were conducted at 60 °C for entries 1-7 in each step; <sup>b</sup> The 1st step was performed at room temperature and 2nd step at 80 °C for entry 8.

#### *Substrate study and plausible mechanism for the sequential conversion of DHPMs to 2-amino-4-arylpyrimidines (5)*

By utilising the above optimized conditions, various pyrimidine derivatives were synthesized from 3, 4-dihydropyrimidinone derivatives obtained through the three component reaction of various aryl aldehydes with ethyl acetoacetate and urea and then condensation with 2, 4-dinitro phenyl hydrazine in acidic medium at high temperature. These results are included in **Table 3B.8**. From this table, we can infer that the nature of various electron donating or withdrawing group containing aryl group at C-4 position of

3, 4-dihydropyrimidinones didn't influence the reaction rate. All the reactions yielded 80-87% of pyrimidine product in 2nd step within 10-15 min at 80 °C. The 2nd step may proceed through activation of carbonyl group for condensation with 2, 4-dinitro phenyl hydrazine in presence of the acid catalyst to form the hydrazone derivatives as reaction intermediate (**Scheme 3B.2**). Under the reaction condition, this intermediate can undergo acid catalyzed aromatization reaction to 2-amino-pyrimidine derivatives with expulsion of 2, 4-dinitroaniline as side product.

**Table 3B.8:** Synthesis of pyrimidine derivatives using [Msim][FeCl<sub>4</sub>]/NaY=0.1 composite as catalyst

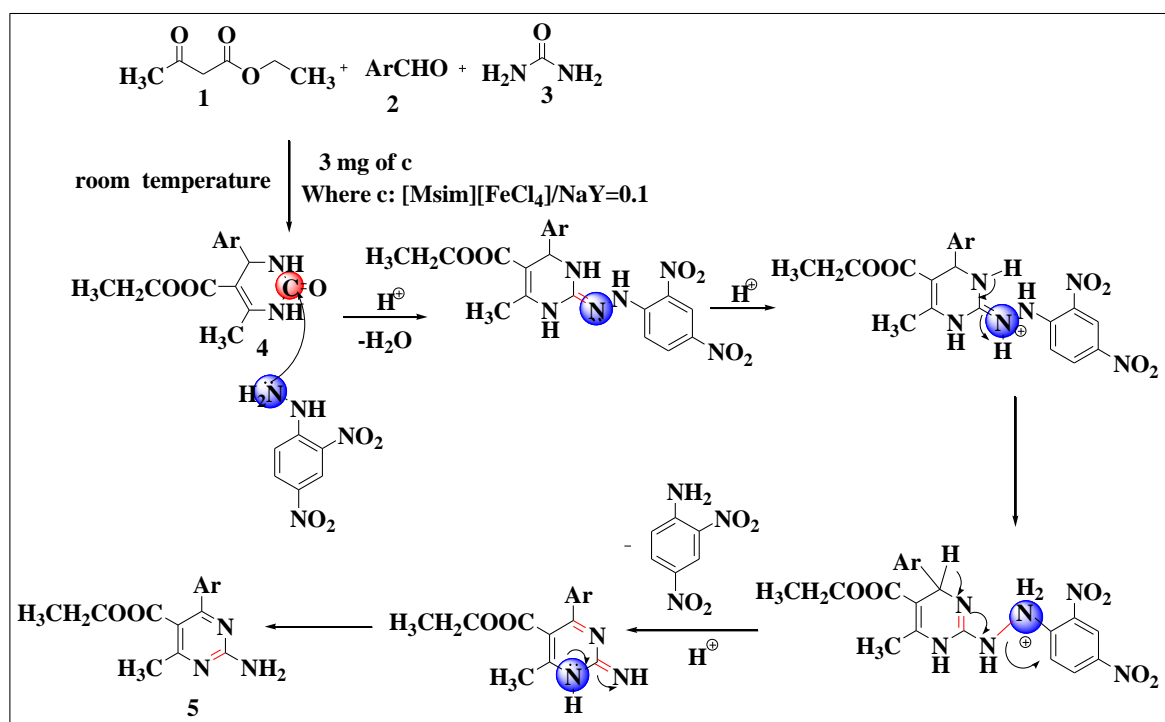
Entry	Aldehyde <b>2</b>	Time(min)		Yield(%) <b>5</b>	M.P. (°C) <b>5</b>
		Step I <sup>a</sup> <b>4</b>	Step II <sup>b</sup> <b>5</b>		
1	C <sub>6</sub> H <sub>5</sub> <b>2a</b>	10	10	87 <b>5a</b>	214.7-217.3
2	4-MeOC <sub>6</sub> H <sub>4</sub> <b>2b</b>	15	10	84 <b>5b</b>	204.8-207.2
3	4-NO <sub>2</sub> C <sub>6</sub> H <sub>4</sub> <b>2c</b>	10	10	82 <b>5c</b>	215.4-217.5
4	4-MeC <sub>6</sub> H <sub>4</sub> <b>2d</b>	15	10	85 <b>5d</b>	227.6-229.4
5	2-Naphthyl <b>2e</b>	20	10	80 <b>5e</b>	163.1-164.0
6	4-HOC <sub>6</sub> H <sub>4</sub> <b>2f</b>	10	10	83 <b>5f</b>	97.4-97.9
7	3,4,5-(MeO) <sub>3</sub> C <sub>6</sub> H <sub>2</sub> <b>2g</b>	10	10	82 <b>5g</b>	158.1-160.5

<sup>a</sup>Reactions were performed at 60 °C using 3 mg of 0.1 composite as catalyst with the mixture of ethyl acetoacetate(1), aromatic aldehyde(2) and urea(3); <sup>b</sup>2,4-Dinitrophenyl hydrazine was added and heated the crude mixture at 80 °C.

#### *Spectral analysis of 2-amino-4-aryl pyrimidine derivatives (5)*

The structures of new 2-amino-4-aryl pyrimidines **5** were confirmed from the <sup>1</sup>H NMR, <sup>13</sup>C NMR, FT-IR and CHN analysis data. Furthermore, two pyrimidines **5a** and **5d** were further studied with COSY, HETCOR and DEPT technique (**Fig. 3B.12-14**). The COSY spectra of both compounds shows two off diagonal cross-peaks for the correlation of triplet at 1.16-1.17 ppm for the -CH<sub>3</sub> group with the quartet peak for -CH<sub>2</sub>- protons at 4.08 ppm of the ester functionality.

The HETCOR spectra of these two compounds assigned the positions of methyl and methylene protons of -COOEt group by their respective cross peaks around 60.0-60.1 ppm and 14.1-14.2 ppm. Similarly, the C-6 methyl singlet at 2.32-2.33 ppm supported its existence with a cross peak at 18.6-18.7 ppm in pyrimidine ring of **5a** and **5d**. The extra methyl substituent present in phenyl ring of **5d** expressed a correlation at 21.1 ppm in the aliphatic region.



**Scheme 3B.2:** Proposed mechanism for one step conversion of Biginelli pyrimidin-2-(1H)-one to 2-amino-4-aryl pyrimidine

The DEPT-45° spectra of the two compounds excluded only the peaks for quaternary carbons while the DEPT-90° spectra indicated the positive signals for -CH-aromatic carbons. For both compounds, the DEPT-135° spectra confirmed the presence of one -CH<sub>2</sub>- group by a negative peak at 4.08 ppm. The same 135° spectra of **5a** and **5d** displayed positive signals in aromatic range for the -CH-carbons and aliphatic region for the -CH<sub>3</sub> groups while no peaks for quaternary carbons.

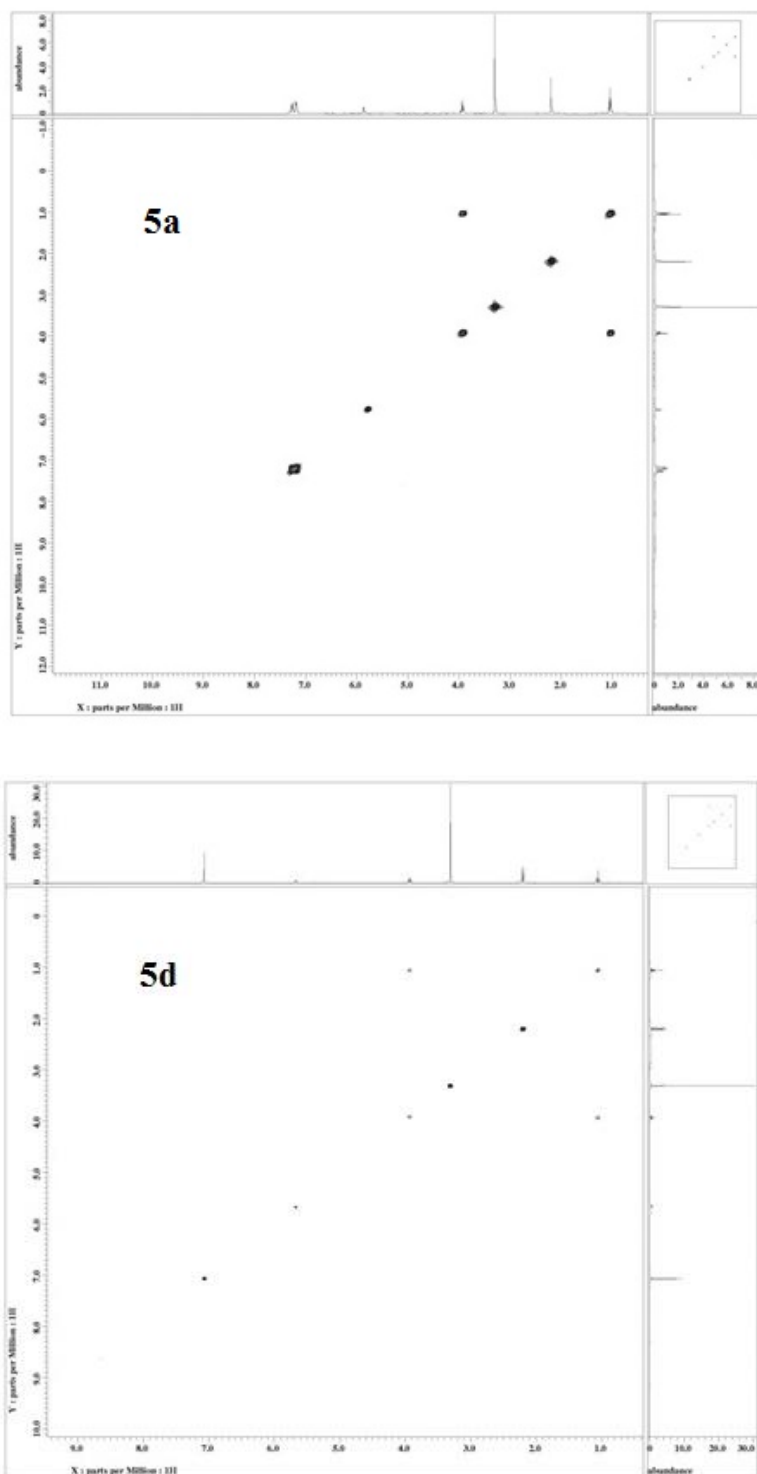


Fig. 3B.12: COSY spectra of 5a & 5d



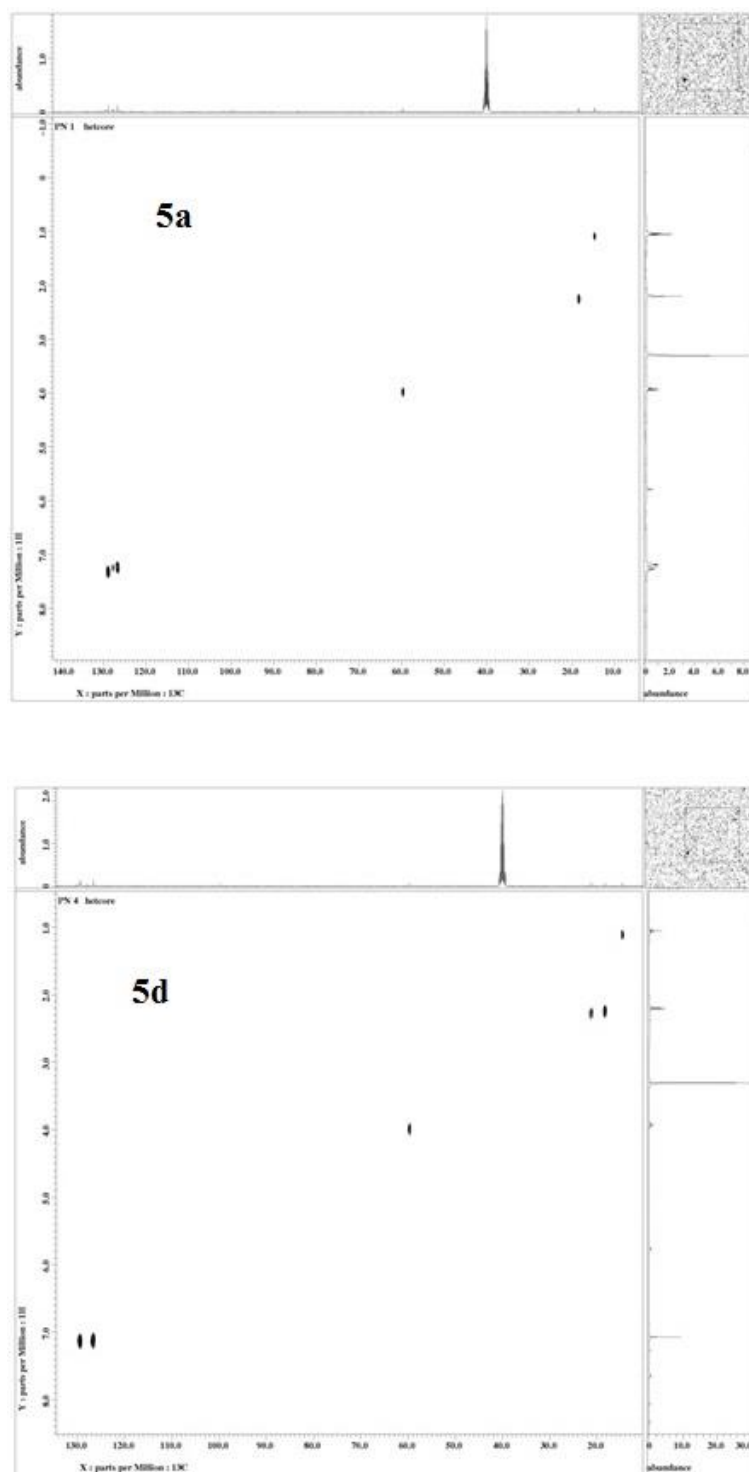


Fig. 3B.13: HETCOR spectra of 5a & 5d

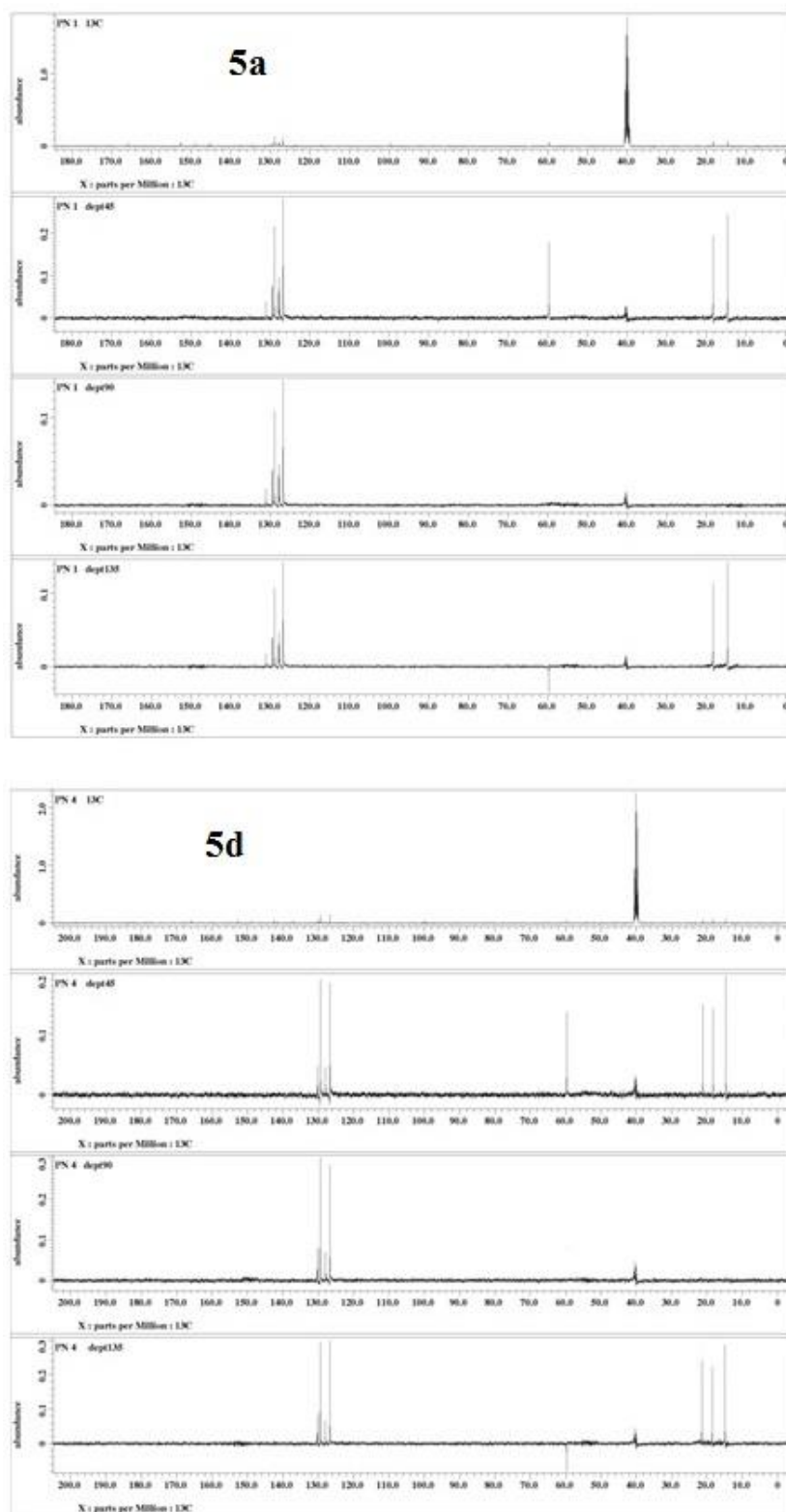
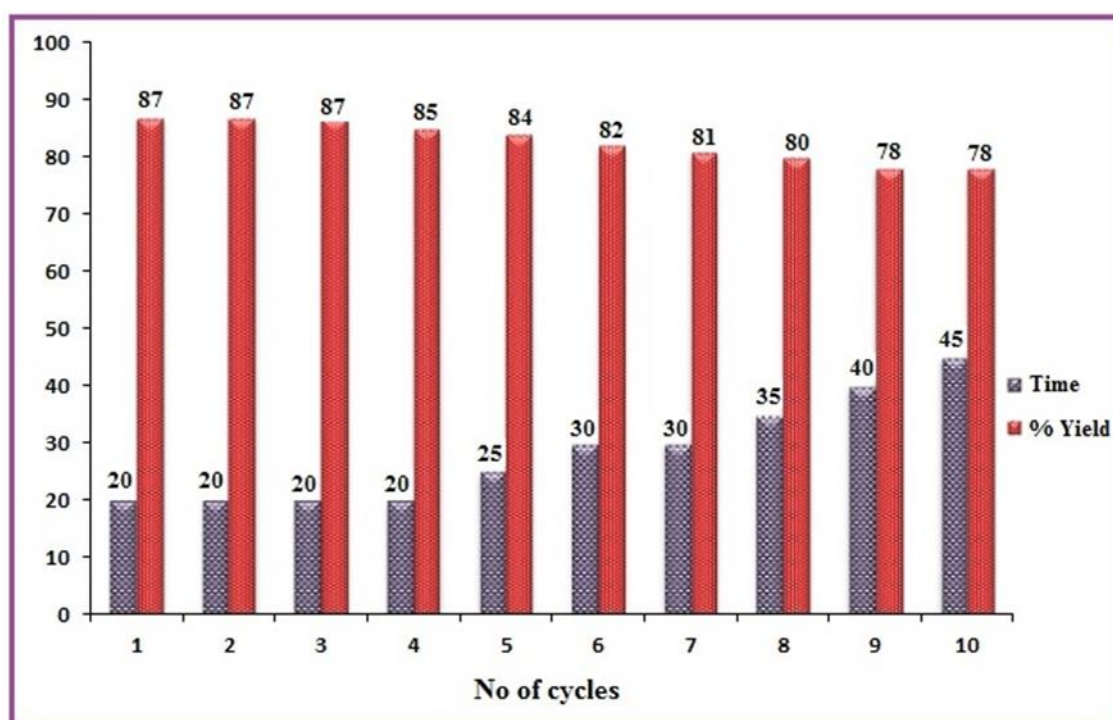


Fig. 3B.14: DEPT 45°, 90° & 135° spectra of 5a & 5d

### Recycling of catalyst

The stability of the active species in supported catalysts is of great concern. The reusability of  $[\text{Msim}][\text{FeCl}_4]/\text{NaY}=0.1$  composite as catalyst was investigated for the one pot synthesis of **5a** under the optimized conditions on a 5mmol scale reaction. The filtered catalyst was repeatedly washed with hot EtOH to make it free from traces of the reaction mixture and then reactivated in vacuum oven at 100 °C for 3 h. The reusability was found to be quite good and it could be reused up to ten consecutive cycles (**Fig. 3B.15**) with moderate loss in activity.



**Fig. 3B.15:** Reusability profile of  $[\text{Msim}][\text{FeCl}_4]/\text{NaY}=0.1$  composite

### Characterization of the used catalyst

The integrity of the used catalyst was checked through FT-IR, Raman spectra and ICP-OES from 2nd cycle onwards after every alternate cycle. FT-IR spectra of the reused catalyst after every alternate cycle from 2nd cycle onwards showed clear evidence of the presence of characteristic bands of the parent zeolite structure as well as the guest ionic solid species (**Fig. 3B.16**). However, the peak characteristic of double ring vibration at  $577\text{ cm}^{-1}$  witnessed slight shifting towards high wavenumber from 2<sup>nd</sup> cycle onwards. From that, we determined the Si/Al ratio of used  $[\text{Msim}][\text{FeCl}_4]/\text{NaY}=0.1$  catalyst from 2<sup>nd</sup> alternate cycle (**Table 3B.9**) using the IR

double-ring ( $\nu_{DR}$ ) vibration values to the empirical relation given by Rüscher et al. [23] with  $Si/Al = (1-x)/x$ .

$$x = 3.857 - 0.00619 \nu_{DR} (\text{cm}^{-1}) \text{-----(2)}$$

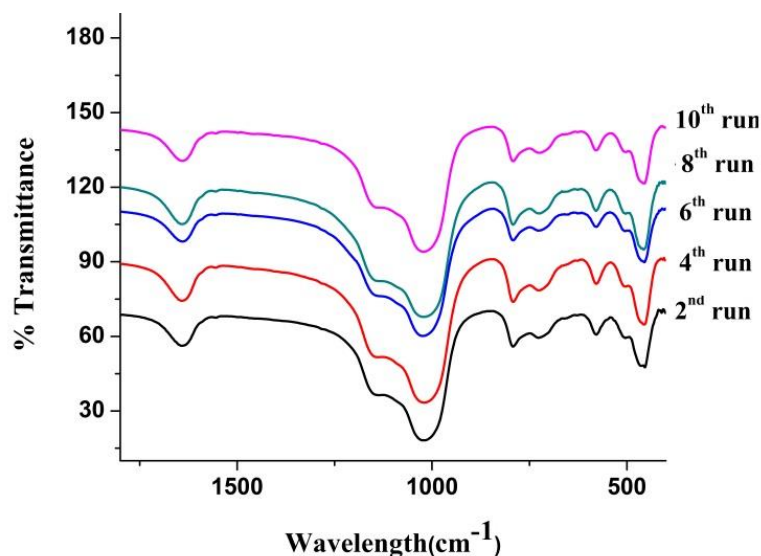


**Fig. 3B.16:** FT-IR spectra of the used catalyst from 2<sup>nd</sup> cycle onwards after every alternate cycle

**Table 3B.9:** Calculation of Si/Al ratio from FT-IR for 0.1(d) (Fresh and reused)

Sample name	Wavenumber(cm-1)	Si/Al ratio
NaY	577.26	2.52
0.1(d) (Fresh)	578.34	2.60
2 <sup>nd</sup> run	578.46	2.61
4 <sup>th</sup> run	578.71	2.64
6 <sup>th</sup> run	578.98	2.66
8 <sup>th</sup> run	579.43	2.70
10 <sup>th</sup> run	579.67	2.72

This table showed the slow leaching of some non-framework Al species to the solution during repeated washing with hot ethanol and then reactivation in vacuum at 100 °C for several hours up to ten consecutive runs. Simultaneously, the ICP-OES results (**Table 3B.10**) also indicated slight loss of Fe content in every alternate cycle after 2<sup>nd</sup> run from the complex anion  $FeCl_4^-$ . The leaching of some non-framework Al

species may destabilize the ionic interaction of  $\text{FeCl}_4^-$  anion with the Lewis acidic site of composite framework. As results, the attached  $\text{FeCl}_4^-$  anion leaches out from the composite to the solution.

**Table 3B.10:** ICP-OES results of the used catalysts

Entry	Cycles	Amount of Fe(mg/L)
1.	2 <sup>nd</sup> cycle	10.23
2.	4 <sup>th</sup> cycle	9.31
3.	6 <sup>th</sup> cycle	7.32
4.	8 <sup>th</sup> cycle	6.92
5.	10 <sup>th</sup> cycle	6.64

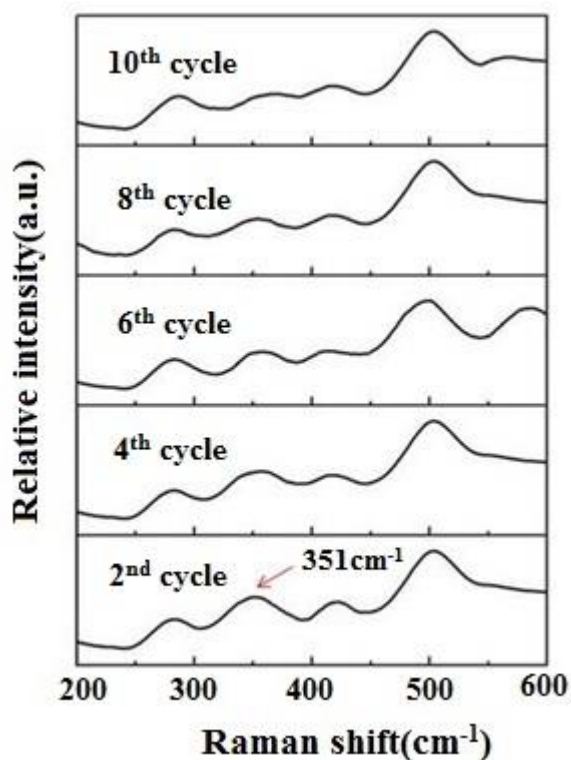


**Fig. 3B.17:** Raman spectra of used catalyst  $[\text{Msim}][\text{FeCl}_4]/\text{NaY} = 0.1$

Raman spectra for the spent catalyst are presented in **Fig. 3B.17**. The intensity of the broad peak at  $351\text{cm}^{-1}$  indicative of  $\text{FeCl}_4^-$  species gradually decreases towards the 10th cycle. It clearly agrees with the leaching information obtained from the ICP-OES study. The respective characterization techniques supports the recyclability diagram for the catalytic system which expressed gradual leaching after 3rd cycle during the repeated washing and reactivation process till the tenth cycle.

### 3B.2. Conclusion

The hybrid composites were characterized with different analytical techniques and they denote the successful entrapment of the ionic solid particles above the NaY zeolite surface. The composite materials are superior in some respects like thermal stability, recyclability etc. than the sole ionic solid. They synergistically combine the advantages of both the host and guest components. Loading up to w/w ratio of 0.2 was found to be the maximum permissible limit. Above this, maximum dealumination caused by presence of higher amount of [Msim][FeCl<sub>4</sub>] over the zeolite surface brought negative effect. The zeolite structure got completely destroyed in case of composites **f** (w/w ratio of 0.5) and **g** (w/w ratio of 1). The [Msim][FeCl<sub>4</sub>]/NaY = 0.1 composite exhibited excellent catalytic activity towards the sequential three component two step conversion of 3, 4-dihydropyrimidin-2(1H)-one to multifunctionalized 2-amino-4-arylpurimidines. The presented methodology proved to be a novel efficient route towards the development of purimidines in less time and would be applicable for the library synthesis of 2-amino-4-arylpurimidine derivatives without using any oxidizing agents and solvents with easy purification.

### 3B.3. Experimental

#### *General techniques*

All chemicals were purchased from different chemical suppliers and used as received without any further treatment. The prepared composites were fully characterized via FT-IR, P-XRD, Raman, SEM-EDX, TEM, TGA, ICP-OES and BET analysis. The synthesized products were characterized via melting point determination, FT-IR, <sup>1</sup>H NMR and <sup>13</sup>C NMR analysis.

#### *Synthesis of NaY supported hybrid catalysts of [Msim][FeCl<sub>4</sub>](b-g)*

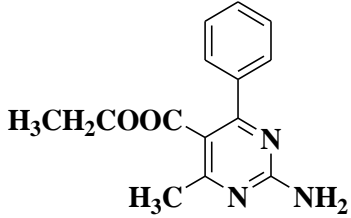
[Msim][FeCl<sub>4</sub>] ionic solid was prepared through a reported procedure [7]. The [Msim][FeCl<sub>4</sub>] loaded NaY zeolite catalysts were prepared by wet impregnation method. The following steps have been utilized: (i) the NaY zeolite powder was out gassed at 600 °C for 3 hour, (ii) [Msim][FeCl<sub>4</sub>] and NaY zeolite were mixed well with six different weight/ weight (w/w) ratios (such as 0.03, 0.05, 0.1, 0.2, 0.5 & 1) of ionic

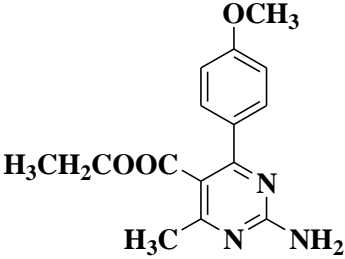
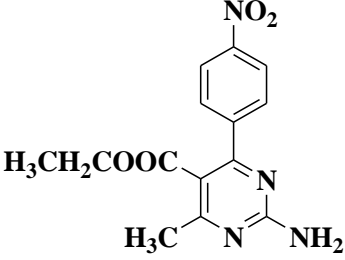
solid and NaY zeolite using few drops of distilled EtOAc to ensure complete mixing, and finally (iii) the mixtures were heated at 150 °C in a vacuum oven for 12 hour.

### **General procedure for the synthesis of 2-amino-4-arylpyrimidine derivatives 5**

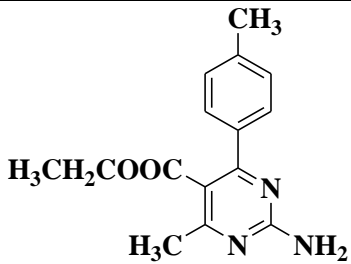
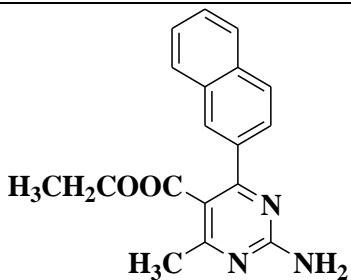
A mixture of ethyl acetoacetate (1 mmol), aromatic aldehyde (1 mmol) and urea (1.5 mmol) was heated in a two necked 50 mL round bottom flask at 60 °C for 10 min using 3 mg of [Msim][FeCl<sub>4</sub>] /NaY= 0.1 catalyst. The formation of 3, 4-dihydropyrimidin-2-(1H)-one was confirmed through thin layer chromatography (TLC) using EtOAc and hexane (1: 3) as solvent system. After completion of the 1st step, 1 mmol of 2, 4-dinitro-phenylhydrazine was added to the crude mixture along with few drops of dichloromethane and heated at 80 °C for the specified time. The progress of 2nd step was also tracked with TLC technique using EtOAc and hexane (1: 5) as developing solvent. The work-up step involved addition of 6 mL of CH<sub>2</sub>Cl<sub>2</sub> to the crude mixture to separate the unreacted DHPMs and catalyst by filtration from the solution of crude pyrimidine. The catalyst was recovered as solid residue on filter paper from the hot solution of DHPMs in ethanol. The saturation of dichloromethane (DCM) solution of pyrimidine at 0 °C precipitated the unreacted 2, 4-dinitro-phenyl hydrazine as red precipitates. Evaporation of DCM solution yielded the pyrimidine derivatives as solid residue which was further recrystallized from acetone and methanol solution.

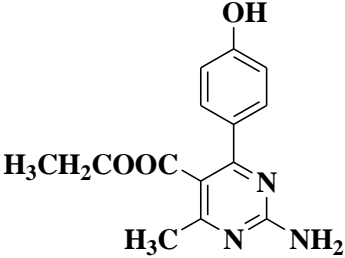
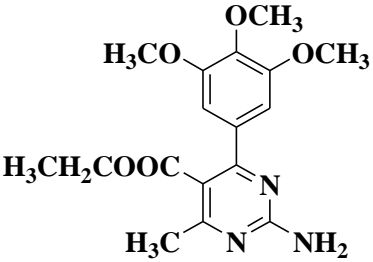
### **3B.4. Spectral data of 2-amino pyrimidine derivatives**

Products	Spectral data
 <p>(Table. 3B.8, entry 1))</p>	<p><b>Ethyl-2-amino-4-phenyl-6-methylpyrimidine-5-carboxylate 5a;</b>            Orange solid; M.P.(°C): 214.7-217.3; FT-IR(KBr) cm<sup>-1</sup>: 3425, 3274, 1699, 1624, 1505, 1422, 1322, 1220, 1126, 759, 690, 614; <sup>1</sup>H NMR (400 MHz, CDCl<sub>3</sub>): δ 7.26-7.31 (m, 5H), 5.81 (s, 2H), 4.08 (q, <i>J</i> = 7.4 Hz, 2H), 2.32 (s, 3H), 1.16 (t, <i>J</i> = 7.4 Hz, 3H); <sup>13</sup>C NMR (100 MHz, CDCl<sub>3</sub>): δ 165.8, 153.4, 147.9, 146.4, 130.1, 129.1, 128.8, 128, 127.7, 101.4, 60.1, 18.7, 14.2;</p>

	CHN analysis(%): C <sub>14</sub> H <sub>15</sub> N <sub>3</sub> O <sub>2</sub> : Cal. C 65.36, H 5.88, N 16.33; Found C 65.34, 5.92, N 16.30.
 <p>(Table. 3B.8, entry 2)</p>	<p><b>Ethyl-2-amino-4-(4-methoxyphenyl)-6-methylpyrimidine-5-carboxylate 5b</b>;  Pink solid; M.P.(°C): 204.8-207.2; FT-IR(KBr) cm<sup>-1</sup>: 3517, 3243, 3114, 2938, 1713, 1649, 1509, 1459, 1281, 1226, 1175, 1092, 1028, 783; <sup>1</sup>H NMR (400 MHz, CDCl<sub>3</sub>): δ 7.22 (d, <i>J</i> = 8.7 Hz, 2H), 6.83 (d, <i>J</i> = 8.7 Hz, 2H), 5.81 (s, 2H), 4.08 (q, <i>J</i> = 7.4 Hz, 2H), 3.78 (s, 3H), 2.33 (s, 3H), 1.18 (t, <i>J</i> = 6.8 Hz, 3H); <sup>13</sup>C NMR (100 MHz, CDCl<sub>3</sub>): δ 165.7, 159.2, 153.4, 145.9, 136.1, 129.3, 127.8, 114.5, 113.9, 101.6, 60.0, 55.1, 18.6, 14.1; CHN analysis(%): C<sub>15</sub>H<sub>17</sub>N<sub>3</sub>O<sub>3</sub>: Cal. C 62.71, H 5.96, N 14.63, Found C 62.68, H 6.03, N 14.57.</p>
 <p>(Table. 3B.8, entry 3)</p>	<p><b>Ethyl-2-amino-4-(4-nitrophenyl)-6-methylpyrimidine-5-carboxylate 5c</b>;  Yellow solid; M.P.(°C): 215.4-217.5; FT-IR(KBr) cm<sup>-1</sup>: 3469, 3232, 3116, 2978, 1708, 1644, 1522, 1462, 1348, 1298, 1220, 1093, 782; <sup>1</sup>H NMR (400 MHz, CDCl<sub>3</sub>): δ 8.16 (d, <i>J</i> = 8.7 Hz, 2H), 7.46 (d, <i>J</i> = 8.7 Hz, 2H), 5.64 (s, 2H), 4.12 (q, <i>J</i> = 7.3Hz, 2H), 2.46 (s, 3H), 1.02 (t, <i>J</i> = 7.3Hz, 3H); <sup>13</sup>C NMR (100 MHz, CDCl<sub>3</sub>): δ 165.7, 152.4, 149.9, 147.2, 128.2, 124.4, 98.8, 60.1, 18.3, 14.5; CHN analysis(%): C<sub>14</sub>H<sub>14</sub>N<sub>4</sub>O<sub>4</sub>: Cal. C 55.63, H 4.67, N 18.53, Found C 55.58, H 4.72, N 18.49.</p>



 <p>(Table. 3B.8, entry 4)</p>	<p><b>Ethyl-2-amino-4-(4-tolyl)-6-methylpyrimidine-5-carboxylate 5d;</b>  Dark pink solid, M.P.(°C) 227.6-229.4;  FT-IR(KBr) <math>\text{cm}^{-1}</math>: 3367, 3247, 3137, 2979, 1708, 1643, 1504, 1462, 1423, 1328, 1224, 1089, 783; <math>^1\text{H}</math> NMR (400 MHz, <math>\text{CDCl}_3</math>): <math>\delta</math> 7.21 (d, <math>J = 8.3</math> Hz, 2H), 7.12 (d, <math>J = 8.2</math> Hz, 2H), 5.76 (s, 2H), 4.08 (q, <math>J = 6.9</math> Hz, 2H), 2.33 (s, 6H), 1.17 (t, <math>J = 7.3</math> Hz, 3H); <math>^{13}\text{C}</math> NMR (100 MHz, <math>\text{CDCl}_3</math>): <math>\delta</math> 165.7, 153.4, 148.1, 146.1, 137.7, 130.0, 129.8, 129.4, 127.6, 126.5, 101.5, 60.0, 21.1, 18.6, 14.1; CHN analysis(%): <math>\text{C}_{15}\text{H}_{17}\text{N}_3\text{O}_2</math>: Cal. C 66.4, H 6.32, N 15.49, Found C 66.32, H 6.38, N 15.43.</p>
 <p>(Table. 3B.8, entry 5)</p>	<p><b>Ethyl-2-amino-4-(naphthalen-3-yl)-6-methylpyrimidine-5-carboxylate 5e;</b>  Yellow solid; M.P.(°C): 163.1-164.0; FT-IR(KBr) <math>\text{cm}^{-1}</math>: 3306, 3228, 3101, 2979, 1721, 1617, 1511, 1426, 1333, 1289, 1211, 1087, 1022, 917, 743; <math>^1\text{H}</math> NMR (400 MHz, <math>\text{CDCl}_3</math>): <math>\delta</math> 8.31(d, <math>J = 9.4</math> Hz, 1H), 7.96 (d, <math>J = 9.2</math> Hz, 1H), 7.77-7.79 (m, 2H), 7.71 (s, 1H), 7.47 (d, <math>J = 9.2</math> Hz, 2H), 5.87 (s, 2H), 4.23 (q, <math>J = 7.4</math> Hz, 2H), 2.17 (s, 3H), 1.31 (t, <math>J = 7.4</math> Hz, 3H); <math>^{13}\text{C}</math> NMR (100 MHz, <math>\text{CDCl}_3</math>): <math>\delta</math> 169.4, 165.7, 153.4, 145.0, 138.2, 133.0, 130.1, 128.9, 128.1, 127.7, 126.3, 125.2, 123.5, 101.3, 61.5, 18.8, 14.3; CHN analysis(%): <math>\text{C}_{18}\text{H}_{17}\text{N}_3\text{O}_2</math>: Cal. C 70.34, H 5.58, N 13.67, Found C 70.26, H 5.64, N 13.65.</p>

 <p>(Table. 3B.8, entry 6)</p>	<p><b>Ethyl-2-amino-4-(4-hydroxyphenyl)-6-methylpyrimidine-5-carboxylate 5f;</b> Light yellow solid; M.P.(°C): 97.4-97.9; FT-IR(KBr) <math>\text{cm}^{-1}</math>: 3388, 3308, 2986, 1728, 1617, 1513, 1426, 1336, 1286, 1204, 1128, 1086, 1024, 919, 733; <math>^1\text{H}</math> NMR (400 MHz, <math>\text{CDCl}_3</math>): <math>\delta</math> 8.32 (d, <math>J = 7.4</math> Hz, 2H), 7.95 (d, <math>J = 7.3</math> Hz, 2H), 4.22 (q, <math>J = 7.4</math> Hz, 2H), 3.47 (s, 2H), 2.15 (s, 3H), 1.29 (t, <math>J = 7.3</math> Hz, 3H); <math>^{13}\text{C}</math> NMR (100 MHz, <math>\text{CDCl}_3</math>): <math>\delta</math> 169.3, 166.9, 150.8, 145.1, 138.3, 130.1, 129.9, 129.5, 123.5, 116.6, 61.5, 16.2, 14.2; CHN analysis(%): <math>\text{C}_{14}\text{H}_{15}\text{N}_3\text{O}_3</math>: Cal. C 61.53, H 5.53, N 15.38, Found C 61.52, H 5.56, N 15.34.</p>
 <p>(Table. 3B.8, entry 7)</p>	<p><b>Ethyl-2-amino-4-(3,4,5-trimethoxyphenyl)-6-methylpyrimidine-5-carboxylate 5g;</b> Dark red solid; M.P.(°C): 158.1-160.5; FT-IR(KBr) <math>\text{cm}^{-1}</math>: 3429, 3311, 3251, 3104, 2977, 1727, 1617, 1513, 1427, 1336, 1289, 1205, 1127, 1089, 1024, 919, 832, 734; <math>^1\text{H}</math> NMR (400 MHz, <math>\text{CDCl}_3</math>): <math>\delta</math> 6.53 (s, 2H), 5.82 (s, 2H), 4.10 (d, <math>J = 6.9</math> Hz, 2H), 3.82 (s, 9H), 2.35 (s, 3H), 1.30 (t, <math>J = 6.9</math> Hz, 3H); <math>^{13}\text{C}</math> NMR (100 MHz, <math>\text{CDCl}_3</math>): <math>\delta</math> 169.4, 165.8, 153.4, 153.3, 150.8, 146.2, 130.1, 104.8, 103.5, 101.3, 60.9, 56.1, 55.9, 18.8, 14.3; CHN analysis(%): <math>\text{C}_{17}\text{H}_{21}\text{N}_3\text{O}_5</math>: Cal. C 58.78, H 6.09, N 12.10, Found C 58.76, H 6.13, N 12.09.</p>

---

**References**

1. Kerr, G. T. Chemistry of crystalline aluminosilicates. V. Preparation of aluminum-deficient faujasites. *The Journal of Physical Chemistry*, 72(7):2594-2596, 1968.
2. Barrer, R. M. and Makki, M. B. Molecular sieve sorbents from clinoptilolite. *Canadian Journal of Chemistry*, 42(6):1481-1487, 1964.
3. Lohse, U., Löffler, E., Hunger, M., Stöckner, J., and Patzelova, V. Hydroxyl groups of the non-framework aluminium species in dealuminated Y zeolites. *Zeolites*, 7(1):11-13, 1987.
4. Maher, P. K., Hunter, F. D., and Scherzer, J. Crystal structures of ultrastable faujasites, *Molecular Sieve Zeolites-I*, pages 266-278, W. R. Grace & Co., Washington Research Center, Clarksville, Md., 1971.
5. Wang, Q. L., Giannetto, G., Torrealba, M., Perot, G., Kappenstein, C., and Guisnet, M. Dealumination of zeolites II. Kinetic study of the dealumination by hydrothermal treatment of a  $\text{NH}_4\text{NaY}$  zeolite. *Journal of Catalysis*, 130(2):459-470, 1991.
6. Salman, N., Rüscher, C.H., Buhl, J.C., Lutz, W., Toufar, H., and Stöcker, M. Effect of temperature and time in the hydrothermal treatment of HY zeolite. *Microporous and Mesoporous materials*, 90(1):339-346, 2006.
7. Gogoi, P., Dutta, A. K., Sarma, P., and Borah, R. Development of Brønsted–Lewis acidic solid catalytic system of 3-methyl-1-sulfonic acid imidazolium transition metal chlorides for the preparation of bis(indolyl) methanes. *Applied Catalysis A: General*, 492:133-139, 2015.
8. Silverstein, R. M. and Webster, F. X. *Spectrometric Identification of Organic Compounds*, Wiley Publisher, 6th edition, 2007.
9. Flanigan, E. M., Khatami, H., and Szymanski, H. A. Infrared structural studies of zeolite frameworks, In Flanigen, E.M. and Sand, L.B., editors, *Molecular Sieve Zeolites- I*, volume 101 of Advances in Chemistry, pages 201–229, American Chemical Society, Washington, DC, 1974.
10. Yan, Z., Ma, D., Zhuang, J., Liu, X., Liu, X., Han, X., Bao, X., Chang, F., Xu, L., and Liu, Z. On the acid-dealumination of USY zeolite: a solid state NMR investigation. *Journal of Molecular Catalysis A: Chemical*, 194(1):153-167, 2003.

11. Covarrubias, C., Quijada, R., and Rojas, R. Ethylene polymerization using dealuminated ZSM-2 zeolite nanocrystals as an active metallocene catalyst support. *Applied Catalysis A: General*, 347(2):223-233, 2008.
12. Qin, Z., Shen, B., Yu, Z., Deng, F., Zhao, L., Zhou, S., Yuan, D., Gao, X., Wang, B., Zhao, H., and Liu, H. A defect-based strategy for the preparation of mesoporous zeolite Y for high-performance catalytic cracking. *Journal of Catalysis*, 298:102-111, 2013.
13. Kerr, G. T. Intracrystalline rearrangement of constitutive water in hydrogen zeolite Y. *The Journal of Physical Chemistry*, 71(12):4155-4156, 1967.
14. Kerr, G. T. Chemistry of crystalline aluminosilicates: VII. Thermal decomposition products of ammonium zeolite Y. *Journal of Catalysis*, 15(2):200-204, 1969.
15. Alwash, A. H., Abdullah, A. Z., and Ismail, N. Elucidation of reaction behaviors in sonocatalytic decolorization of amaranth dye in water using Zeolite Y co-incorporated with Fe and TiO<sub>2</sub>. *Advances in Chemical Engineering and Science*, 3(02):113-122, 2013.
16. Valtchev, V., Majano, G., Mintova, S., and Pérez-Ramírez, J. Tailored crystalline microporous materials by post-synthesis modification. *Chemical Society Reviews*, 42(1):263-290, 2013.
17. Senderov, E., Halasz, I., and Olson, D. H. On existence of hydroxyl nests in acid dealuminated zeolite Y. *Microporous and Mesoporous Materials*, 186:94-100, 2014.
18. Grobet, P. J., Jacobs, P. A., and Beyer, H. K. Study of the silicon tetrachloride dealumination of NaY by a combination of NMR and IR methods. *Zeolites*, 6(1):47-50, 1986.
19. Fejes, P., Hannus, I., Kiricsi, I., Pfeifer, H., Freude, D., and Oehme, W. Thermal stability of hydroxy groups in dealuminated mordenites. *Zeolites*, 5(1):45-48, 1985.
20. Dutta, P. K., Shieh, D. C., and Puri, M. Correlation of framework Raman bands of zeolites with structure. *Zeolites*, 8(4):306-309, 1988.
21. Ntais, S., Moschovi, A., Dracopoulos, V., and Nikolakis, V. Ionic liquid/zeolite composites: synthesis and characterization using vibrational spectroscopy techniques. *ECS Transactions*, 33(7):41-47, 2010.

22. Hajipour, A. R. and Rafiee, F. Acidic Brønsted ionic liquids. *Organic Preparations and Procedures International*, 42(4):285-362, 2010.
23. Rüscher, C. H., Buhl, J. -C., Lutz, W. In Galarneau, A., Di Renzo, F., Fajula, F., and Vedrine J., editors, *Studies in Surface Science and Catalysis*, volume 135, pages 13-15, Elsevier, Amsterdam, 2001.